Available online at www.sciencedirect.com
SCIENCE DIRECT®
Journal of Computational Physics 199 (2004) 175–204
JOURNAL OF COMPUTATIONAL PHYSICS
www.elsevier.com/locate/jcp

Asymptotic equilibrium diffusion analysis of time-dependent Monte Carlo methods for grey radiative transfer

Jeffery D. Densmore [a,*], Edward W. Larsen [b]

[a] *Transport Methods Group, Los Alamos National Laboratory, Los Alamos, NM 87545, USA*
[b] *Department of Nuclear Engineering and Radiological Sciences, University of Michigan, Ann Arbor, MI 48109, USA*

Received 30 May 2003; received in revised form 5 January 2004; accepted 10 February 2004
Available online 5 March 2004

Abstract

The equations of nonlinear, time-dependent radiative transfer are known to yield the equilibrium diffusion equation as the leading-order solution of an asymptotic analysis when the mean-free path and mean-free time of a photon become small. We apply this same analysis to the Fleck–Cummings, Carter–Forest, and N'kaoua Monte Carlo approximations for grey (frequency-independent) radiative transfer. Although Monte Carlo simulation usually does not require the discretizations found in deterministic transport techniques, Monte Carlo methods for radiative transfer require a time discretization due to the nonlinearities of the problem. If an asymptotic analysis of the equations used by a particular Monte Carlo method yields an accurate time-discretized version of the equilibrium diffusion equation, the method should generate accurate solutions if a time discretization is chosen that resolves temperature changes, even if the time steps are much larger than the mean-free time of a photon. This analysis is of interest because in many radiative transfer problems, it is a practical necessity to use time steps that are large compared to a mean-free time. Our asymptotic analysis shows that: (i) the N'kaoua method has the equilibrium diffusion limit, (ii) the Carter–Forest method has the equilibrium diffusion limit if the material temperature change during a time step is small, and (iii) the Fleck–Cummings method does not have the equilibrium diffusion limit. We include numerical results that verify our theoretical predictions.

Keywords: Radiative transfer; Monte Carlo; Asymptotic analysis

1. Introduction

Asymptotic analysis has been shown to be a powerful technique for analyzing discrete-ordinates spatial-differencing methods for linear transport problems in optically thick, diffusive media [1]. In this technique,

* Corresponding author. Tel.: +1-505-665-9198.
E-mail addresses: jdd@lanl.gov (J.D. Densmore), edlarsen@engin.umich.edu (E.W. Larsen).

0021-9991/$ - see front matter © 2004 Elsevier Inc. All rights reserved.
doi:10.1016/j.jcp.2004.02.004

asymptotic solutions to the discrete equations are generated as the mean-free path becomes small, the spatial grid is fixed, and the spatial cells become optically thick. The analytic transport equation yields the diffusion equation in this asymptotic limit [2–4], and it is desirable for the discretized transport equation to yield a discretized version of the correct limiting diffusion equation. If the leading-order discrete asymptotic solution yields a valid discretization of the diffusion equation, the transport discretization method is said to have the *diffusion limit*. Discrete-ordinate methods that have this limit yield accurate results for diffusive problems, even if the spatial cells are not optically thin. If the discrete method does not have the diffusion limit, an optically thin spatial grid must be employed to achieve an accurate solution, even if the solution varies slowly with respect to the spatial variable [5,6].

A similar asymptotic limit exists for the nonlinear, time-dependent thermal radiative transfer equations, yielding the *equilibrium diffusion equation* [7]. In this limit, both the mean-free path and mean-free time of a photon become small. Several discrete-ordinate methods for radiative transfer have been analyzed asymptotically using this approach [8,9].

Monte Carlo methods are also used to solve thermal radiative transfer problems [10–12]. Unlike linear transport problems, in which Monte Carlo solutions can be generated virtually free of truncation error, Monte Carlo methods for radiative transfer are "linearized" over each time step. This linearization is required to treat the nonlinear dependence of material properties on the temperature. Especially troublesome is the fact that the material itself is a nonlinear source of photons, due to Planckian emission [13]. For stability reasons, the processes of photon absorption, increase or decrease in material temperature, and photon emission within the time step are usually treated in an implicit or semi-implicit manner. In fact, the distinction between the different Monte Carlo methods is their implicit approximation to the absorption–reemission process. However, even when an "implicit" approximation to the emission source is used, unphysical solutions may be generated if large time steps are employed [14–16].

In this paper, we perform an asymptotic equilibrium diffusion limit analysis of three Monte Carlo methods for thermal radiative transfer: the Fleck–Cummings method [10], the Carter–Forest method [11], and the N'kaoua method [12]. If this analysis yields, to leading order, a valid discretization of the equilibrium diffusion equation, we say that the method has the *equilibrium diffusion limit*. In this limit, the mean-free path and mean-free time of a photon become small, the time discretization is fixed, and the time steps become optically large (i.e., large compared to a mean-free time). This analysis is of interest in problems that approach the equilibrium diffusion limit, where it is often too computationally expensive to employ time steps that are small with respect to the mean-free time. We propose that if a Monte Carlo method has the equilibrium diffusion limit, accurate results will be obtained for problems with diffusive characteristics, even if large time steps with respect to the mean-free time are used. (However, the time-step size must be adequate to resolve the diffusion solution. Accurate results will not be achieved if the time step is *too* large.) If a method does not have the equilibrium diffusion limit, to obtain an accurate solution, optically small time steps must be employed.

There are a few caveats regarding the scope of this paper. First, we consider radiative transfer in the grey (frequency-independent) case only. Although Monte Carlo simulation does not require a multigroup discretization of the frequency variable, the linearization process used by the Monte Carlo method introduces errors into the frequency spectrum of the solution because the spectrum of a Planckian emission source is a function of the material temperature, which is usually held constant during the time step in a Monte Carlo simulation. This constant-temperature approximation may yield incorrect results in the equilibrium diffusion limit. Secondly, although Monte Carlo simulations have statistical errors, our analysis treats only "ideal" solutions to the underlying linearized equations that are free from statistical error. Finally, in most Monte Carlo implementations, the physical system is subdivided into a spatial grid, with material properties and temperature constant within each spatial cell. For simplicity, we treat the material temperature as a continuous function in space. The focus of this paper is the analysis of errors introduced in Monte Carlo simulations of grey radiative transfer problems by various time-

discretization schemes; we do not consider spatial truncation errors here, but we discuss this issue more thoroughly in our conclusions section.

We begin the remainder of this paper with a description of the equations of radiative transfer and the corresponding equilibrium diffusion equation. Then, we briefly overview the Monte Carlo methods of interest and present the results of an asymptotic analysis for each of these methods. This analysis generates a time-differenced equation for each Monte Carlo method, which we compare to a time discretization of the equilibrium diffusion equation. Finally, we present and discuss numerical results for relevant problems with diffusive properties.

2. Analytical equations

In the absence of internal sources and scattering, the grey radiative transfer equations are [13]

$$\frac{1}{c}\frac{\partial I}{\partial t} + \vec{\Omega}\cdot\vec{\nabla} I = \sigma\left(\frac{1}{4\pi} acT^4 - I\right) \tag{1}$$

and

$$\frac{\partial U_{\mathrm{m}}}{\partial t} = \sigma\left(\int I \,\mathrm{d}\Omega - acT^4\right). \tag{2}$$

Here $\vec{r}$ is the spatial variable, $\vec{\Omega}$ is the angular variable, t is the time variable, $I(\vec{r},\vec{\Omega},t)$ is the radiation intensity, $T(\vec{r},t)$ is the material temperature, $\sigma(\vec{r},T)$ is the opacity, a is the radiation constant, and c is the speed of light. We assume local thermodynamic equilibrium, in which the emission source is a Planckian at the local material temperature:

$$\frac{1}{4\pi}\sigma acT^4. \tag{3}$$

The material temperature T and the material energy density, $U_{\mathrm{m}}(\vec{r},t)$ are related by

$$\frac{\partial U_{\mathrm{m}}}{\partial T} = C_{\mathrm{v}} > 0, \tag{4}$$

where $C_{\mathrm{v}}(\vec{r},T)$ is the heat capacity. Thus, the material energy density is an explicit function of temperature, $U_{\mathrm{m}}[T(\vec{r},t)]$. The left-hand side of Eq. (2) can then be written in terms of temperature,

$$\frac{\partial U_{\mathrm{m}}}{\partial t} = C_{\mathrm{v}}\frac{\partial T}{\partial t}. \tag{5}$$

An equilibrium solution exists for Eqs. (1) and (2), in which the radiation intensity is a Planckian at the material temperature:

$$I = \frac{1}{4\pi} acT^4. \tag{6}$$

To complete the problem description, we impose initial conditions for I and T at $t = 0$,

$$I(\vec{r},\vec{\Omega},0) = I_i(\vec{r},\vec{\Omega}), \tag{7}$$

$$T(\vec{r},0) = T_i(\vec{r}), \tag{8}$$

and a boundary condition that specifies I on the outer boundary of the system for incoming directions. Since the focus of this paper is on time discretization schemes, we do not consider boundary conditions explicitly.

We consider the following scaling of Eqs. (1) and (2):

$$\frac{\epsilon^2}{c}\frac{\partial I}{\partial t} + \epsilon\vec{\Omega}\cdot\vec{\nabla}I = \sigma\left(\frac{1}{4\pi}acT^4 - I\right), \tag{9}$$

$$\epsilon^2 C_{\mathrm{v}}\frac{\partial T}{\partial t} = \epsilon^2\frac{\partial U_{\mathrm{m}}}{\partial t} = \sigma\left(\int I\,\mathrm{d}\Omega - acT^4\right), \tag{10}$$

where $\epsilon \ll 1$. Larsen et al. [7] give a physical justification for this scaling. However, we note that it can be achieved by allowing (i) the opacity to become large ($\sigma \to \sigma/\epsilon$), (ii) the heat capacity to become small ($C_{\mathrm{v}} \to \epsilon C_{\mathrm{v}}$), and (iii) the speed of light on the left-hand side of Eq. (1) to become large ($c \to c/\epsilon$). Physically, this represents a system in which the mean-free path is $\mathrm{O}(\epsilon)$ when compared to the length scale over which I and T vary by $\mathrm{O}(1)$, the mean-free time is $\mathrm{O}(\epsilon^2)$ when compared to the time scale over which I and T vary by $\mathrm{O}(1)$, and $\mathrm{O}(\epsilon)$ amounts of radiation energy absorbed and emitted by the material correspond to $\mathrm{O}(1)$ changes in the material temperature. For consistency, we have also scaled the material energy density in Eq. (10) (i.e. $U_{\mathrm{m}} \to \epsilon U_{\mathrm{m}}$). This scaling, as $\epsilon \to 0$, is known as the *equilibrium diffusion limit*.

Eqs. (9) and (10) are the starting point for an asymptotic analysis. Larsen et al. [7] have shown that, away from boundaries and initial times, as $\epsilon \to 0$, the leading-order intensity is a Planckian at the local temperature,

$$I^{(0)} = \frac{1}{4\pi}ac(T^{(0)})^4, \tag{11}$$

and the leading-order temperature satisfies the following nonlinear diffusion equation:

$$\frac{\partial}{\partial t}U_{\mathrm{m}}(T^{(0)}) + a\frac{\partial}{\partial t}(T^{(0)})^4 = \vec{\nabla}\cdot\frac{ac}{3\sigma}\vec{\nabla}(T^{(0)})^4. \tag{12}$$

If we define the *radiation flux* as

$$\vec{F} = \int \vec{\Omega}I\,\mathrm{d}\Omega, \tag{13}$$

then the rate of spatial flow of radiation energy is $-\vec{\nabla}\cdot\vec{F}$. From Eq. (11), there is no leading-order flux, but the $\mathrm{O}(\epsilon)$ flux is given by Fick's law [7]:

$$\vec{F}^{(1)} = -\frac{ac}{3\sigma}\vec{\nabla}(T^{(0)})^4. \tag{14}$$

Eq. (12) is then a statement of conservation of energy: the left-hand side is the time rate of change in the material and radiation energy, and the right-hand side represents the spatial flow of radiation energy.

Pomraning [17] has performed an initial-layer analysis to determine an initial condition for Eq. (12). This initial condition requires $T^{(0)}(\vec{r},0)$ to satisfy the nonlinear equation

$$U_{\mathrm{m}}\left[T^{(0)}(\vec{r},0)\right] + a\left[T^{(0)}(\vec{r},0)\right]^4 = U_{\mathrm{m}}[T_i(\vec{r})] + \frac{1}{c}\int I_i(\vec{r},\vec{\Omega})\,\mathrm{d}\Omega. \tag{15}$$

Eq. (15) combines the initial material and radiation energy densities such that material and radiation are locally in equilibrium at $T^{(0)}(\vec{r},0)$.

3. Overview of Monte Carlo methods

To develop a Monte Carlo method for radiative transfer, we must first "linearize" Eqs. (1) and (2). We begin by defining a fixed temporal grid $0 = t_0 < t_1 < t_2 < \cdots$. Within each time step $t_n \leqslant t \leqslant t_{n+1}$, a time-dependent Monte Carlo simulation is performed of a linearized problem, with initial conditions generated by the previous time step, or by the initial conditions, Eqs. (7) and (8), if $n = 0$. The Monte Carlo-calculated radiation intensity can then be used to update the material energy density, and in turn the material temperature. In most Monte Carlo methods the material energy density and temperature are calculated as an average over a spatial cell, with temperature-dependent quantities being considered constant within each spatial cell and calculated with the appropriate cell-averaged temperature. We do not explicitly show this spatial discretization in the following paragraphs, except where necessary for clarity.

We begin linearizing Eqs. (1) and (2) by approximating the opacity as constant within each time step,

$$\sigma(T) \approx \sigma_n, \tag{16}$$

where σ_n can be defined at the temperature at the end of the previous time step, or at some extrapolated temperature within the current time step. In addition, we define the *equilibrium* radiation energy density as

$$U_{\mathrm{r}} = aT^4. \tag{17}$$

Eqs. (1) and (2) can then be written for $t_n \leqslant t \leqslant t_{n+1}$ as

$$\frac{1}{c}\frac{\partial I}{\partial t} + \vec{\Omega}\cdot\vec{\nabla} I = \sigma_n\left(\frac{1}{4\pi}cU_{\mathrm{r}} - I\right) \tag{18}$$

and

$$\frac{\partial U_{\mathrm{m}}}{\partial t} = \sigma_n\left(\int I\,\mathrm{d}\Omega - cU_{\mathrm{r}}\right). \tag{19}$$

The following Monte Carlo methods differ in their approximation to U_{r} within the time step.

3.1. The Fleck–Cummings method

To derive the Fleck–Cummings method [10], we rewrite the left-hand side of Eq. (19) as

$$\frac{\partial U_{\mathrm{m}}}{\partial t} = \frac{\partial U_{\mathrm{m}}}{\partial T}\frac{\partial T}{\partial U_{\mathrm{r}}}\frac{\partial U_{\mathrm{r}}}{\partial t} = \frac{1}{\beta}\frac{\partial U_{\mathrm{r}}}{\partial t}, \tag{20}$$

where, employing Eqs. (4) and (17),

$$\beta = \frac{\partial T}{\partial U_{\mathrm{m}}}\frac{\partial U_{\mathrm{r}}}{\partial T} = \frac{4aT^3}{C_{\mathrm{v}}}. \tag{21}$$

Approximating β by its beginning of time-step value,

$$\beta(T) \approx \beta(T_n) = \beta_n, \tag{22}$$

where T_n is the temperature calculated at the end of the previous time step, we may write Eq. (19) as

$$\frac{1}{\beta_n}\frac{\partial U_{\mathrm{r}}}{\partial t} = \sigma_n\left(\int I\,\mathrm{d}\Omega - cU_{\mathrm{r}}\right). \tag{23}$$

Integrating Eq. (23) over the time step, we obtain

$$U_{\mathrm{r},n+1} = aT_n^4 + \sigma_n\beta_n \int_{t_n}^{t_{n+1}} \left(\int I \,\mathrm{d}\Omega - cU_\mathrm{r} \right) \mathrm{d}t, \tag{24}$$

where the subscript n denotes the value at time t_n, as in Eq. (22). In Eq. (24) $U_{\mathrm{r},n+1}$ is an approximation to U_r at the end of the current time step ($U_{\mathrm{r},n+1} \neq aT_{n+1}^4$). We now approximate the step-averaged value of U_r by interpolating between the beginning and end of time-step values,

$$\frac{1}{\Delta t_n} \int_{t_n}^{t_{n+1}} U_\mathrm{r} \,\mathrm{d}t = \tilde{U}_\mathrm{r} = \alpha U_{\mathrm{r},n+1} + (1-\alpha) aT_n^4, \tag{25}$$

where $\Delta t_n = t_{n+1} - t_n$, and α is a parameter chosen by the user, usually taken between 1/2 and 1. Eqs. (24) and (25) yield

$$U_{\mathrm{r},n+1} = f_n \left\{ [1-(1-\alpha)\beta_n c\sigma_n \Delta t_n] aT_n^4 + \beta_n \sigma_n \int_{t_n}^{t_{n+1}} \int I \,\mathrm{d}\Omega \,\mathrm{d}t \right\}, \tag{26}$$

where the *Fleck factor* f_n is defined as

$$f_n = \frac{1}{1+\alpha\beta_n c\sigma_n \Delta t_n}. \tag{27}$$

Eqs. (25) and (26) then yield the average value of U_r over the time step:

$$\tilde{U}_\mathrm{r} = f_n aT_n^4 + \alpha\beta_n\sigma_n f_n \int_{t_n}^{t_{n+1}} \int I \,\mathrm{d}\Omega \,\mathrm{d}t. \tag{28}$$

The following time-dependent approximation for U_r within the timestep is consistent with Eq. (28):

$$U_\mathrm{r} \approx f_n aT_n^4 + \alpha\beta_n\sigma_n\Delta t_n f_n \int I \,\mathrm{d}\Omega. \tag{29}$$

Substituting Eq. (29) into Eq. (18), we obtain the Fleck–Cummings transport equation

$$\frac{1}{c}\frac{\partial I}{\partial t} + \vec{\Omega}\cdot\vec{\nabla} I + \sigma_n I = \frac{1}{4\pi}\sigma_n(1-f_n) \int I(\vec{r},\vec{\Omega}',t)\,\mathrm{d}\Omega' + \frac{1}{4\pi}\sigma_n f_n acT_n^4. \tag{30}$$

This is a standard linear transport equation, which can be solved for $t_n \leqslant t \leqslant t_{n+1}$ using a Monte Carlo simulation. To approximate the absorption–reemission process, Eq. (30) includes an artificial scattering term (representing photons absorbed and reemitted within the time step),

$$\frac{1}{4\pi}\sigma_n(1-f_n) \int I(\vec{r},\vec{\Omega}',t)\,\mathrm{d}\Omega', \tag{31}$$

and a source term (representing photons absorbed in previous time steps and reemitted during the current time step),

$$\frac{1}{4\pi}\sigma_n f_n acT_n^4. \tag{32}$$

To update the material energy density (and temperature), we approximate U_r in Eq. (19) by Eq. (29). Integrating Eq. (19) over the time step, we obtain

$$U_{\mathrm{m}}(T_{n+1}) = U_{\mathrm{m}}(T_n) + \sigma_n f_n \int_{t_n}^{t_{n+1}} \int I \,\mathrm{d}\Omega \,\mathrm{d}t - \sigma_n f_n \Delta t_n a c T_n^4. \tag{33}$$

Once $U_{\mathrm{m}}(T_{n+1})$ has been calculated, the end of time-step temperature T_{n+1} is calculated using the nonlinear equation

$$U_{\mathrm{m}}(T_{n+1}) - U_{\mathrm{m}}(T_n) = \int_{T_n}^{T_{n+1}} C_{\mathrm{v}}(T) \,\mathrm{d}T, \tag{34}$$

which is obtained from Eq. (4).

3.2. The Carter–Forest method

To derive the Carter–Forest method [11], Eq. (19) is approximated by Eq. (23), just as in the derivation of the Fleck–Cummings method. The starting point for the Carter–Forest method is then Eqs. (18) and (23):

$$\frac{1}{c}\frac{\partial I}{\partial t} + \vec{\Omega}\cdot\vec{\nabla} I = \sigma_n \left(\frac{1}{4\pi} c U_{\mathrm{r}} - I \right), \tag{35}$$

$$\frac{\partial U_{\mathrm{r}}}{\partial t} = \sigma_n \beta_n \left(\int I \,\mathrm{d}\Omega - c U_{\mathrm{r}} \right). \tag{36}$$

However, instead of approximating an average value of U_{r}, one solves Eq. (36) exactly, yielding

$$U_{\mathrm{r}}(t) = a T_n^4 \,\mathrm{e}^{-c\sigma_n\beta_n(t-t_n)} + \int_{t_n}^{t} \int \sigma_n \beta_n \,\mathrm{e}^{-c\sigma_n\beta_n(t-t')} I(\vec{r}, \vec{\Omega}, t') \,\mathrm{d}\Omega \,\mathrm{d}t'. \tag{37}$$

Using Eqs. (37) and (35), the Carter–Forest transport equation then becomes

$$\frac{1}{c}\frac{\partial I}{\partial t} + \vec{\Omega}\cdot\vec{\nabla} I + \sigma_n I = \frac{1}{4\pi} c\sigma_n \left[a T_n^4 \,\mathrm{e}^{-c\sigma_n\beta_n(t-t_n)} + \int_{t_n}^{t} \int \sigma_n \beta_n \,\mathrm{e}^{-c\sigma_n\beta_n(t-t')} I(\vec{r}, \vec{\Omega}', t') \,\mathrm{d}\Omega' \,\mathrm{d}t' \right]. \tag{38}$$

Eq. (38) represents the absorption–reemission process by including a time-dependent "reemission" term (representing photons that are absorbed and reemitted during the time step),

$$\frac{1}{4\pi} \int_{t_n}^{t} \int c\sigma_n \beta_n \,\mathrm{e}^{-c\sigma_n\beta_n(t-t')} \sigma_n I(\vec{r}, \vec{\Omega}', t') \,\mathrm{d}\Omega' \,\mathrm{d}t' \tag{39}$$

and a time-dependent "source" term (representing photons absorbed in previous time steps and emitted during the current step),

$$\frac{1}{4\pi} \sigma_n a c T_n^4 \,\mathrm{e}^{-c\sigma_n\beta_n(t-t_n)}. \tag{40}$$

Eq. (39) represents a process in which photons are absorbed, then reemitted at a later time isotropically. The probability distribution function for the reemission time is

$$c\sigma_n\beta_n \,\mathrm{e}^{-c\sigma_n\beta_n(t-t')}, \tag{41}$$

where t' is the absorption time and t is the reemission time. In standard implementations of the Carter–Forest method, particles that would be reemitted past the end of the time step are considered absorbed and added to the material energy (this energy is then emitted exponentially in the following time step).

To update the material energy density, Eq. (37) is substituted into the right-hand side of Eq. (19), and the resultant equation is integrated over the time step. This yields

$$U_{\mathrm{m}}(T_{n+1}) = U_{\mathrm{m}}(T_n) + \int_{t_n}^{t_{n+1}} \int \sigma_n \mathrm{e}^{-c\sigma_n\beta_n(t_{n+1}-t)} I(\vec{r},\vec{\Omega},t)\,\mathrm{d}\Omega\,\mathrm{d}t - \frac{aT_n^4}{\beta_n}\left(1-\mathrm{e}^{-c\sigma_n\beta_n\Delta t_n}\right). \tag{42}$$

As with the Fleck–Cummings method, Eq. (34) is solved for the end of time-step temperature once $U_{\mathrm{m}}(T_{n+1})$ is determined. The only approximations in the Carter–Forest method are that the nonlinear terms σ and β are held constant within a time step (and that, in practice, a spatial grid is used to represent the material temperature and any temperature-dependent material properties).

3.3. The N'kaoua method

Instead of using Eq. (19) to develop an approximation for U_{r}, the N'kaoua method approximates U_{r} in Eqs. (18) and (19) by its end of time-step value [12]. The starting point for this method is

$$\frac{1}{c}\frac{\partial I}{\partial t} + \vec{\Omega}\cdot\vec{\nabla} I + \sigma_n I = \frac{1}{4\pi}\sigma_n acT_{n+1}^4 \tag{43}$$

and

$$\frac{\partial U_{\mathrm{m}}}{\partial t} = \sigma_n \int I\,\mathrm{d}\Omega - \sigma_n acT_{n+1}^4. \tag{44}$$

The key to the N'kaoua method is noting that Eq. (43) can be solved for I (as a function of T_{n+1}) without knowing T_{n+1}. The Monte Carlo simulation is accomplished by treating the weights of the particles as unknowns. This technique is similar to one proposed by Brooks [18] for line transport (i.e., local thermodynamic equilibrium is not assumed). After I is calculated, Eq. (44) can be solved for T_{n+1}.

We briefly overview the implementation of the N'kaoua method. To begin, we subdivide the transport problem into several problems. The first problem is given by

$$\frac{1}{c}\frac{\partial I_0}{\partial t} + \vec{\Omega}\cdot\vec{\nabla} I_0 + \sigma_n I_0 = 0, \tag{45}$$

with initial condition

$$I_0(\vec{r},\vec{\Omega},t_n) = I(\vec{r},\vec{\Omega},t_n), \tag{46}$$

which is known from the results of the previous time step. Eq. (45) should also account for any external radiation sources. This transport problem represents particles with known weights. Then, for each spatial cell j, we define the problem

$$\frac{1}{c}\frac{\partial I_j}{\partial t} + \vec{\Omega}\cdot\vec{\nabla} I_j + \sigma_n I_j = \frac{1}{4\pi}\sigma_n c\chi_j, \tag{47}$$

$$I_j(\vec{r},\vec{\Omega},t_n) = 0, \tag{48}$$

where χ_j is unity in cell j, and vanishes in all other cells. In Eq. (47), U_{r} has been set to unity within the cell of interest. This transport problem accounts for particles emitted by each spatial cell during the current step.

After I_0 and I_j for each cell are determined, the results are used to evaluate the integral on the right-hand side of Eq. (44), and the resulting equation is integrated over the timestep (and the jth spatial cell). This yields

$$U_{\mathrm{m}}(T_{n+1,j}) = U_{\mathrm{m}}(T_{n,j}) + \frac{1}{V_j}\int_{t_n}^{t_{n+1}} \int\int_j \sigma_{n,j} I_0 \,\mathrm{d}^3 r \,\mathrm{d}\Omega \,\mathrm{d}t + \sum_k \left(\frac{1}{V_j}\int_{t_n}^{t_{n+1}} \int\int_j \sigma_{n,j} I_k \,\mathrm{d}^3 r \,\mathrm{d}\Omega \,\mathrm{d}t \right) a T_{n+1,k}^4 - \sigma_{n,j}\Delta t_n a c T_{n+1,j}^4, \tag{49}$$

where V_j is the volume of cell j, $\sigma_{n,j}$ is the opacity of cell j, and $T_{n+1,j}$ is the temperature at the end of the time step in cell j. Eq. (49), along with Eq. (34), for all cells j, constitutes a system of nonlinear equations that is solved for $T_{n+1,j}$.

The N'kaoua method differs from the other Monte Carlo methods in that, from Eq. (49), it is truly nonlinear. No linearization process, as used in the Fleck–Cummings and Carter–Forest methods, is employed in the derivation of the N'kaoua method (i.e., $\beta = 4aT^3/C_{\mathrm{v}}$ is not held constant during the time step). However, the opacity is held constant over a time step, as in the other Monte Carlo methods, so the N'kaoua method does have a linearization error in problems with temperature-dependent opacities. Also, the N'kaoua method approximates the emission source implicitly, which yields a truncation error.

4. Asymptotic analysis

We now present an asymptotic analysis for each of the above methods within a time step. This analysis generates a difference equation for T_n that is a (hopefully valid) time-discretized version of the equilibrium diffusion equation, Eq. (12). The asymptotic analysis also generates expressions similar to Eqs. (11) and (15).

We begin by applying the approximations discussed in the previous section to Eqs. (9) and (10). Then, away from the beginning of the time step, we express the radiation intensity and temperature as interior solutions,

$$I = I^{(\mathrm{i})}(\vec{r}, \vec{\Omega}, t) \tag{50}$$

and

$$T = T^{(\mathrm{i})}(\vec{r}, t). \tag{51}$$

Near the beginning of the time step, the radiation intensity and temperature are given by initial-layer solutions,

$$I = I^{(\mathrm{il})}(\vec{r}, \vec{\Omega}, t, \tau) \tag{52}$$

and

$$T = T^{(\mathrm{il})}(\vec{r}, t, \tau), \tag{53}$$

where we have defined the "fast" time variable as

$$\tau = \frac{t - t_n}{\epsilon^2}. \tag{54}$$

In this analysis, t and τ are considered independent variables, and we treat the temperature as a continuous function of $\vec{r}$.

The initial-layer solutions are subject to initial conditions,

$$I^{(\mathrm{il})}(\vec{r},\vec{\Omega},t_n,0) = I(\vec{r},\vec{\Omega},t_n) \tag{55}$$

and

$$T^{(\mathrm{il})}(\vec{r},t_n,0) = T(\vec{r},t_n), \tag{56}$$

where $I(\vec{r},\vec{\Omega},t_n)$ and $T(\vec{r},t_n)$ are provided by the results of the previous time step. The following matching conditions link the initial-layer and interior solutions:

$$\lim_{\tau\to\infty} I^{(\mathrm{il})}(\vec{r},\vec{\Omega},t,\tau) = I^{(\mathrm{i})}(\vec{r},\vec{\Omega},t), \tag{57}$$

$$\lim_{\tau\to\infty} T^{(\mathrm{il})}(\vec{r},t,\tau) = T^{(\mathrm{i})}(\vec{r},t). \tag{58}$$

Eqs. (57) and (58) effectively provide initial conditions for the interior solutions. This multiple scale technique described above was used by Larsen et al. [7] to asymptotically derive the equilibrium diffusion equation.

4.1. The N'kaoua method

Applying the approximation used in the N'kaoua method to Eqs. (9) and (10), the equations for the interior solution are

$$\frac{\epsilon^2}{c}\frac{\partial I^{(\mathrm{i})}}{\partial t} + \epsilon\vec{\Omega}\cdot\vec{\nabla}I^{(\mathrm{i})} + \sigma_n I^{(\mathrm{i})} = \frac{1}{4\pi}\sigma_n ac\left(T^{(\mathrm{i})}_{n+1}\right)^4 \tag{59}$$

and

$$\epsilon^2\frac{\partial}{\partial t}U_{\mathrm{m}}\left(T^{(\mathrm{i})}\right) = \sigma_n\left[\int I^{(\mathrm{i})}\,\mathrm{d}\Omega - ac\left(T^{(\mathrm{i})}_{n+1}\right)^4\right]. \tag{60}$$

We have not subdivided Eq. (59) into separate transport problems, or integrated Eq. (60) over the time step, in order to make the following analysis easier. Next, we expand the radiation intensity and material temperature into power series of ϵ:

$$I^{(\mathrm{i})} = \sum_k \epsilon^k I^{(\mathrm{i},k)} \tag{61}$$

and

$$T^{(\mathrm{i})} = \sum_k \epsilon^k T^{(\mathrm{i},k)}. \tag{62}$$

The temperature-dependent terms in Eqs. (59) and (60) can also be expanded into a power series in ϵ. For example, the material energy density can be written as

$$U_{\mathrm{m}} = U^{(0)}_{\mathrm{m}} + \epsilon U^{(1)}_{\mathrm{m}} + \epsilon^2 U^{(2)}_{\mathrm{m}} + \cdots, \tag{63}$$

where

$$U^{(0)}_{\mathrm{m}} = U_{\mathrm{m}}\big|_{\epsilon=0} = U_{\mathrm{m}}\left(T^{(\mathrm{i},0)}\right), \tag{64}$$

$$U_{\mathrm{m}}^{(1)} = \left.\frac{\partial U_{\mathrm{m}}}{\partial \epsilon}\right|_{\epsilon=0} = \left.\frac{\partial U_{\mathrm{m}}}{\partial T}\frac{\partial T}{\partial \epsilon}\right|_{\epsilon=0} = C_{\mathrm{v}}\left(T^{(\mathrm{i},0)}\right)T^{(\mathrm{i},1)} \tag{65}$$

and

$$\begin{aligned} U_{\mathrm{m}}^{(2)} &= \left.\frac{1}{2}\frac{\partial^2 U_{\mathrm{m}}}{\partial \epsilon^2}\right|_{\epsilon=0} = \left.\frac{1}{2}\left[\frac{\partial^2 U_{\mathrm{m}}}{\partial T^2}\left(\frac{\partial T}{\partial \epsilon}\right)^2 + \frac{\partial U_{\mathrm{m}}}{\partial T}\frac{\partial T^2}{\partial \epsilon^2}\right]\right|_{\epsilon=0} \\ &= \frac{1}{2}\left[\left.\frac{\partial^2 U_{\mathrm{m}}}{\partial T^2}\right|_{T=T^{(\mathrm{i},0)}}\left(T^{(\mathrm{i},1)}\right)^2 + C_{\mathrm{v}}\left(T^{(\mathrm{i},0)}\right)T^{(\mathrm{i},2)}\right]. \end{aligned} \tag{66}$$

We are now in a position to analyze Eqs. (59) and (60) by comparing terms that are the same order in ϵ.

The O(1) equations are

$$\sigma_n^{(0)} I^{(\mathrm{i},0)} = \frac{1}{4\pi}\sigma_n^{(0)} ac\left(T_{n+1}^{(\mathrm{i},0)}\right)^4 \tag{67}$$

and

$$0 = \sigma_n^{(0)}\left[\phi^{(\mathrm{i},0)} - ac\left(T_{n+1}^{(\mathrm{i},0)}\right)^4\right]. \tag{68}$$

Here, we have defined the kth-order angularly integrated intensity as

$$\phi^{(\mathrm{i},k)} = \int I^{(\mathrm{i},k)}\,\mathrm{d}\Omega. \tag{69}$$

Eq. (67) yields

$$I^{(\mathrm{i},0)} = \frac{1}{4\pi} ac\left(T_{n+1}^{(\mathrm{i},0)}\right)^4, \tag{70}$$

which is consistent with Eq. (68). Thus, the leading-order interior radiation intensity is a Planckian of the local leading-order temperature at the end of the time step. This is an implicit approximation to Eq. (11). We also note that, to leading order, the interior radiation flux is zero

$$\vec{F}^{(\mathrm{i},0)} = \int \vec{\Omega} I^{(\mathrm{i},0)}\,\mathrm{d}\Omega = 0. \tag{71}$$

The O(ϵ) equations are

$$\vec{\Omega}\cdot\vec{\nabla} I^{(\mathrm{i},0)} + \sigma_n^{(0)} I^{(\mathrm{i},1)} = \frac{1}{4\pi}\sigma_n^{(0)} c U_{\mathrm{r}}^{(1)}\left(T_{n+1}^{(\mathrm{i})}\right) \tag{72}$$

and

$$0 = \sigma_n^{(0)}\left[\phi^{(\mathrm{i},1)} - cU_{\mathrm{r}}^{(1)}\left(T_{n+1}^{(\mathrm{i})}\right)\right]. \tag{73}$$

From Eqs. (70) and (72) the O(ϵ) intensity is

$$I^{(\mathrm{i},1)} = -\frac{ac}{4\pi\sigma_n^{(0)}}\vec{\Omega}\cdot\vec{\nabla}\left(T_{n+1}^{(\mathrm{i},0)}\right)^4 + \frac{1}{4\pi} cU_{\mathrm{r}}^{(1)}\left(T_{n+1}^{(\mathrm{i})}\right), \tag{74}$$

which is consistent with Eq. (73). The O(ϵ) interior radiation flux is given by

$$\vec{F}^{(\mathrm{i},1)} = -\frac{ac}{3\sigma_n^{(0)}}\vec{\nabla}\left(T_{n+1}^{(\mathrm{i},0)}\right)^4, \tag{75}$$

which is equivalent to Eq. (14).

The $\mathrm{O}(\epsilon^2)$ equations are

$$\frac{1}{c}\frac{\partial I^{(\mathrm{i},0)}}{\partial t} + \vec{\Omega}\cdot\vec{\nabla}I^{(\mathrm{i},1)} + \sigma_n^{(0)}I^{(\mathrm{i},2)} + \sigma_n^{(1)}I^{(\mathrm{i},1)} = \frac{1}{4\pi}c\left[\sigma_n^{(0)}U_{\mathrm{r}}^{(2)}\left(T_{n+1}^{(\mathrm{i})}\right) + \sigma_n^{(1)}U_{\mathrm{r}}^{(1)}\left(T_{n+1}^{(\mathrm{i})}\right)\right] \tag{76}$$

and

$$\frac{\partial}{\partial t}U_{\mathrm{m}}^{(0)}\left(T^{(\mathrm{i})}\right) = \sigma_n^{(0)}\left[\phi^{(\mathrm{i},2)} - cU_{\mathrm{r}}^{(2)}\left(T_{n+1}^{(\mathrm{i})}\right)\right]. \tag{77}$$

Using Eqs. (70) and (74), we integrate Eq. (76) over all directions, yielding

$$-\vec{\nabla}\cdot\frac{ac}{3\sigma_n^{(0)}}\vec{\nabla}\left(T_{n+1}^{(\mathrm{i},0)}\right)^4 + \sigma_n^{(0)}\phi^{(\mathrm{i},2)} = \sigma_n^{(0)}cU_{\mathrm{r}}^{(2)}\left(T_{n+1}^{(\mathrm{i})}\right). \tag{78}$$

Then, using Eq. (78), we integrate Eq. (77) from t_n to t_{n+1}, resulting in

$$\frac{U_{\mathrm{m}}\left(T_{n+1}^{(\mathrm{i},0)}\right) - U_{\mathrm{m}}\left[T^{(\mathrm{i},0)}(\vec{r},t_n)\right]}{\Delta t_n} = \vec{\nabla}\cdot\frac{ac}{3\sigma_n^{(0)}}\vec{\nabla}\left(T_{n+1}^{(\mathrm{i},0)}\right)^4. \tag{79}$$

This is a diffusion-like equation for the leading-order interior temperature at the end of the time step, $T_{n+1}^{(\mathrm{i},0)}$. We must now perform an initial-layer analysis to determine an initial condition for the leading-order interior temperature, $T^{(\mathrm{i},0)}(\vec{r},t_n)$.

The equations for the initial layer are

$$\frac{\epsilon^2}{c}\frac{\partial I^{(\mathrm{il})}}{\partial t} + \frac{1}{c}\frac{\partial I^{(\mathrm{il})}}{\partial \tau} + \epsilon\vec{\Omega}\cdot\vec{\nabla}I^{(\mathrm{il})} + \sigma_n I^{(\mathrm{il})} = \frac{1}{4\pi}\sigma_n ac\left(T_{n+1}^{(\mathrm{i})}\right)^4 \tag{80}$$

and

$$\epsilon^2\frac{\partial}{\partial t}U_{\mathrm{m}}\left(T^{(\mathrm{il})}\right) + \frac{\partial}{\partial\tau}U_{\mathrm{m}}\left(T^{(\mathrm{il})}\right) = \sigma_n\left[\int I^{(\mathrm{il})}\,\mathrm{d}\Omega - ac\left(T_{n+1}^{(\mathrm{i})}\right)^4\right]. \tag{81}$$

Using a similar expansion for the initial-layer temperature and intensity as was done in Eqs. (61) and (62), the $\mathrm{O}(1)$ equations are

$$\frac{1}{c}\frac{\partial I^{(\mathrm{il},0)}}{\partial\tau} + \sigma_n^{(0)}I^{(\mathrm{il},0)} = \frac{1}{4\pi}\sigma_n^{(0)}ac\left(T_{n+1}^{(\mathrm{i},0)}\right)^4 \tag{82}$$

and

$$\frac{\partial}{\partial\tau}U_{\mathrm{m}}\left(T^{(\mathrm{il},0)}\right) = \sigma_n^{(0)}\left[\phi^{(\mathrm{il},0)} - ac\left(T_{n+1}^{(\mathrm{i},0)}\right)^4\right]. \tag{83}$$

Integrating Eq. (82) over all directions and adding the results to Eq. (83), we obtain

$$\frac{1}{c}\frac{\partial\phi^{(\mathrm{il},0)}}{\partial\tau} + \frac{\partial}{\partial\tau}U_{\mathrm{m}}\left(T^{(\mathrm{il},0)}\right) = 0. \tag{84}$$

Next, letting $t = t_n$, integrating from $\tau = 0$ to $\tau = \infty$, and using Eqs. (55)–(58) and (70), Eq. (84) becomes

$$a\left(T_{n+1}^{(\mathrm{i},0)}\right)^4 - \frac{1}{c}\int I^{(0)}(\vec{r},\vec{\Omega},t_n)\,\mathrm{d}\Omega + U_{\mathrm{m}}\left[T^{(\mathrm{i},0)}(\vec{r},t_n)\right] - U_{\mathrm{m}}\left[T^{(0)}(\vec{r},t_n)\right] = 0, \tag{85}$$

where $I^{(0)}(\vec{r},\vec{\Omega},t_n)$ and $T^{(0)}(\vec{r},t_n)$ are the leading-order initial conditions generated by the previous time step for the radiation intensity and material temperature, respectively. Eq. (85) now gives an effective initial condition for $T^{(\mathrm{i},0)}(\vec{r},t_n)$.

Using Eq. (85), Eq. (79) can be written as

$$\frac{U_{\mathrm{m}}\left(T_{n+1}^{(\mathrm{i},0)}\right) - U_{\mathrm{m}}\left[T^{(0)}(\vec{r},t_n)\right]}{\Delta t_n} + \frac{1}{\Delta t_n}a\left(T_{n+1}^{(\mathrm{i},0)}\right)^4 - \frac{1}{\Delta t_n c}\int I^{(0)}(\vec{r},\vec{\Omega},t_n)\,\mathrm{d}\Omega = \vec{\nabla}\cdot\frac{ac}{3\sigma_n^{(0)}}\vec{\nabla}\left(T_{n+1}^{(\mathrm{i},0)}\right)^4. \tag{86}$$

For all but the first time step, the leading-order initial conditions are given by the leading-order interior solutions at the end of the previous time step:

$$T^{(0)}(\vec{r},t_n) = T_n^{(\mathrm{i},0)}, \tag{87}$$

$$I^{(0)}(\vec{r},\vec{\Omega},t_n) = \frac{1}{4\pi}ac\left(T_n^{(\mathrm{i},0)}\right)^4. \tag{88}$$

Eq. (86) then becomes, for all but the first time step,

$$\frac{U_{\mathrm{m}}\left(T_{n+1}^{(\mathrm{i},0)}\right) - U_{\mathrm{m}}\left(T_n^{(\mathrm{i},0)}\right)}{\Delta t_n} + a\frac{\left(T_{n+1}^{(\mathrm{i},0)}\right)^4 - \left(T_n^{(\mathrm{i},0)}\right)^4}{\Delta t_n} = \vec{\nabla}\cdot\frac{ac}{3\sigma_n^{(0)}}\vec{\nabla}\left(T_{n+1}^{(\mathrm{i},0)}\right)^4. \tag{89}$$

Eq. (89) is a valid implicit discretization of Eq. (12), the equilibrium diffusion equation. For the first time step, Eq. (89) will still hold if we define $T_n^{(\mathrm{i},0)}$ for $n = 0$ by

$$U_{\mathrm{m}}\left(T_0^{(\mathrm{i},0)}\right) + a\left(T_0^{(\mathrm{i},0)}\right)^4 = U_{\mathrm{m}}(T_i) + \frac{1}{c}\int I_i\,\mathrm{d}\Omega, \tag{90}$$

where T_i and I_i are given by Eqs. (7) and (8). Eq. (90) is identical to Eq. (15), the initial condition for the equilibrium diffusion equation described by Pomraning [17].

In summary, an asymptotic analysis of the N'kaoua method yields, to leading order, a valid (implicit) discretization of the equilibrium diffusion equation, Eq. (89). In addition, the leading-order radiation intensity is given by a Planckian at the local end of time-step temperature, Eq. (70), and the initial condition for the leading-order temperature, Eq. (90), is identical to the initial condition for the equilibrium diffusion equation. Thus, the N'kaoua method has the equilibrium diffusion limit.

4.2. The Fleck–Cummings method

Next, we present the results of an asymptotic analysis of the Fleck–Cummings method. For conciseness, the details of this analysis are given in Appendix A, although the techniques are similar to those used in the analysis of the N'kaoua method.

The equation governing the leading-order interior radiation intensity is

$$\frac{1}{c}\frac{\partial\phi^{(\mathrm{i},0)}}{\partial t} - \vec{\nabla}\cdot\frac{1}{3\sigma_n^{(0)}}\vec{\nabla}\phi^{(\mathrm{i},0)} + \sigma_{\mathrm{a},n}^{(2)}\phi^{(\mathrm{i},0)} = \sigma_{\mathrm{a},n}^{(2)}ac\left(T_n^{(\mathrm{i},0)}\right)^4. \tag{91}$$

Although Eq. (91) is a diffusion-like equation, it is incorrect because it does not require the intensity and temperature to be locally in equilibrium, as in Eq. (11) (i.e. $\phi \neq acT^4$). Thus, the Fleck–Cummings method

does not generate a radiation intensity that is a Planckian at the local material temperature. Also, Eq. (91) has an effective absorption coefficient, $\sigma_{a,n}^{(2)}$, which is not a function of the opacity [see Eq. (A.7) in Appendix A]. This effective absorption coefficient is consistent with the Fleck–Cummings approximation, in which physical absorption and reemission are replaced by pseudo scattering and pseudo absorption in the transport process. In addition, the source term $\sigma_{a,n}^{(2)} ac(T_n^{(i,0)})^4$ is evaluated using the temperature from the previous time step, which may cause difficulties if large time steps are employed.

From an initial-layer analysis, there is no initial layer at the beginning of a time step, and the end of time-step intensity and material temperature can be employed directly at the beginning of the next time step. The equation governing the interior material temperature is then

$$\frac{U_m\left(T_{n+1}^{(i,0)}\right) - U_m\left(T_n^{(i,0)}\right)}{\Delta t_n} + \frac{1}{c}\frac{\phi_{n+1}^{(i,0)} - \phi_n^{(i,0)}}{\Delta t_n} = \frac{1}{\Delta t_n}\int_{t_n}^{t_{n+1}} \vec{\nabla}\cdot\frac{1}{3\sigma_n^{(0)}}\vec{\nabla}\phi^{(i,0)}(\vec{r},t)\,dt, \tag{92}$$

where $\phi^{(i,0)}(\vec{r},t)$ is defined by Eq. (91), and initial conditions for $n = 0$ are given directly by Eqs. (7) and (8). This is a statement of conservation of energy, where the left-hand side of Eq. (92) is the change in material and radiation energy over the time step, and the right side, the spatial flow of radiation, is given by Fick's law. Although Eq. (92) is similar to Eq. (12), the Fleck–Cummings method does not have the equilibrium diffusion limit since Eq. (11) is not satisfied, nor is there an initial condition similar to Eq. (15). However, it is not clear how poorly the Fleck–Cummings method will perform in problems with diffusive characteristics. Since Eq. (91) is a diffusion equation for the radiation intensity, it is possible that reasonably accurate estimates of the material temperature will be generated, although the intensity and temperature may not be locally in equilibrium. As we will see in the numerical results presented later in this paper, the Fleck–Cummings method is capable of generating reasonable solutions, even when optically-large time steps are used.

4.3. The Carter–Forest method

We now present the results from an asymptotic analysis of the Carter–Forest method. Again, the details of the analysis are given in Appendix A.

The equation governing the leading-order interior intensity is

$$\frac{1}{c}\left(1 + \frac{1}{\beta_n^{(0)}}\right)\frac{\partial\phi^{(i,0)}}{\partial t} = \vec{\nabla}\cdot\frac{1}{3\sigma_n^{(0)}}\vec{\nabla}\phi^{(i,0)}. \tag{93}$$

Although Eq. (93) is a diffusion-like equation, it is incorrect since it does not require the radiation intensity and material temperature to be in local equilibrium, as in Eq. (11). Eq. (93) represents a diffusion process with no absorption and a decreased photon speed. This is consistent with the Carter–Forest approximation, in which the absorption-reemission process has been replaced by photons exiting scattering events at a delayed time, effectively slowing the transport process.

From an initial layer analysis, the initial condition for the leading-order interior intensity is

$$\phi^{(i,0)}(\vec{r},t_n) = \frac{\beta_n^{(0)}}{1+\beta_n^{(0)}}\phi^{(0)}(\vec{r},t_n) + \frac{1}{1+\beta_n^{(0)}}ac\left[T^{(0)}(\vec{r},t_n)\right]^4, \tag{94}$$

where $\phi^{(0)}(\vec{r},t_n)$ and $T^{(0)}(\vec{r},t_n)$ are the end of time-step values for the intensity and temperature from the previous time step, respectively. Eq. (94) has the interpretation of being a weighted average of the leading-order temperature and radiation intensity from the previous time step. Also, the initial condition for the leading-order temperature is

$$U_{\mathrm{m}}\left[T^{(\mathrm{i},0)}(\vec{r},t_n)\right] = U_{\mathrm{m}}\left[T^{(0)}(\vec{r},t_n)\right] + \frac{1}{c}\left[\phi^{(0)}(\vec{r},t_n) - \phi^{(\mathrm{i},0)}(\vec{r},t_n)\right]. \tag{95}$$

These equations are not valid versions of Eq. (15).

The equation for the leading-order interior material temperature is

$$\frac{U_{\mathrm{m}}\left(T_{n+1}^{(\mathrm{i},0)}\right) - U_{\mathrm{m}}\left(T_n^{(\mathrm{i},0)}\right)}{\Delta t_n} + \frac{1}{c}\frac{\phi_{n+1}^{(\mathrm{i},0)} - \phi_n^{(\mathrm{i},0)}}{\Delta t_n} = \frac{1}{\Delta t_n}\int_{t_n}^{t_{n+1}} \vec{\nabla}\cdot\frac{1}{3\sigma_n^{(0)}}\vec{\nabla}\phi^{(\mathrm{i},0)}\,\mathrm{d}t. \tag{96}$$

Eq. (96) is similar to the equilibrium diffusion equation, Eq. (12). It is a statement of conservation of energy, with the change in material and radiation energy balanced by the spatial flow of radiation energy (which is given by Fick's Law). However, in general, the Carter–Forest method does not have the equilibrium diffusion limit since the radiation intensity is given by Eqs. (93) and (94), not Eq. (11), nor is there an initial condition similar to Eq. (15).

However, there is a subset of problems in which the Carter–Forest method nearly yields the equilibrium diffusion limit. If the material temperature does not change by much over a time step, then Eqs. (93)–(96) can be shown to reduce to discrete versions of Eqs. (11), (12) and (15). The details of this analysis are given in Appendix A. Thus, if the time grid is small enough such that the time rate of change of the temperature is resolved, *and* the initial intensity and temperature are nearly in equilibrium, then the Carter–Forest method will generate accurate, physically-correct solutions. We note that this favorable result does not hold for the Fleck–Cummings method.

5. Numerical results

We now present the results from several numerical simulations. In these problems, we use a temperature-independent opacity of $\sigma = 100$ cm^{-1} and a temperature-independent heat capacity of $C_{\mathrm{v}} = 0.01$ GJ/cm^3-keV (1 GJ = 1 gigajoule = 10^9 J). In our problems temperature is measured in keV, and time is measured in ns (1 ns = 1 nanosecond = 10^{-9} s). In these units, the speed of light c is 29.98 cm/ns, and the radiation constant a is 0.01372 GJ/cm^3-keV^4. The mean-free time of a photon, using these physical constants and material properties, is 3.34×10^{-4} ns. We have chosen the opacity and heat capacity above to be consistent with the scaling in Eqs. (9) and (10), and so that the time steps employed in the following problems are many mean-free times long.

We first examine the results of an infinite medium problem in which the material temperature and radiation intensity are initially out of equilibrium. This problem serves to test how well the results of the asymptotic analysis of each method satisfy the initial condition, Eq. (15). Since this problem has no space dependence, no Monte Carlo simulation is required, and the underlying equations in each Monte Carlo method are solved exactly. We employ an implicitness factor of $\alpha = 1$ in the Fleck–Cummings calculations, and a time-step size of $\Delta t = 0.01$ ns, which is much larger than the mean-free time of a photon. Since our calculations do not resolve the initial layer, the best one can hope for is that the Monte Carlo method will generate the equilibrium solution at the end of a single time step. This will happen if an initial condition similar to Eq. (15) is generated in the asymptotic analysis of the Monte Carlo method. Our theoretical results predict that the N'kaoua method has this initial condition, that the Carter–Forest method has this initial condition when the material temperature and radiation intensity are not too far out of equilibrium initially, and that the Fleck–Cummings method never has this initial condition.

The material temperatures calculated by the three Monte Carlo methods are plotted in Figs. 1–3. In these problems, the material temperature is initially set to 0.4 keV, and the radiation intensity is given by a Planckian initially at temperatures $T_R = 0.5$, 0.7, and 1.0 keV. In all three problems, the N'kaoua method

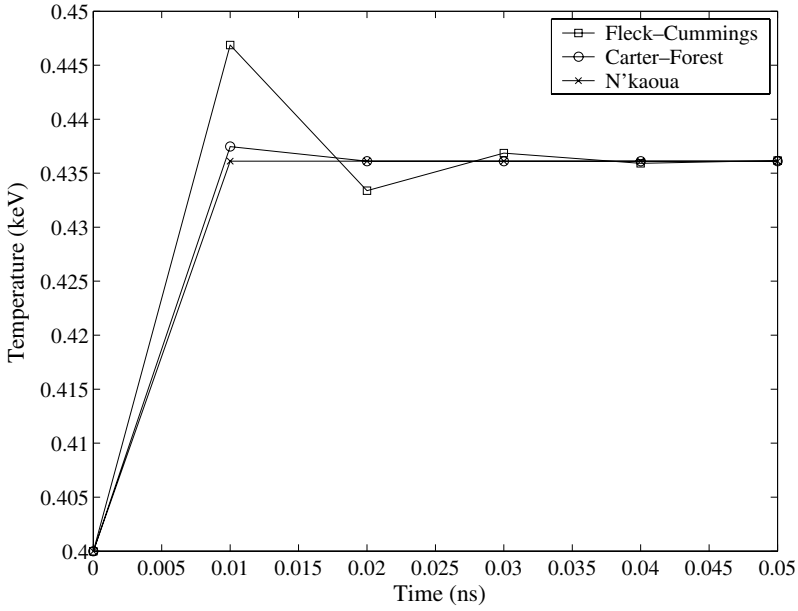

Fig. 1. Infinite medium material temperature, $T_R = 0.5$ keV.

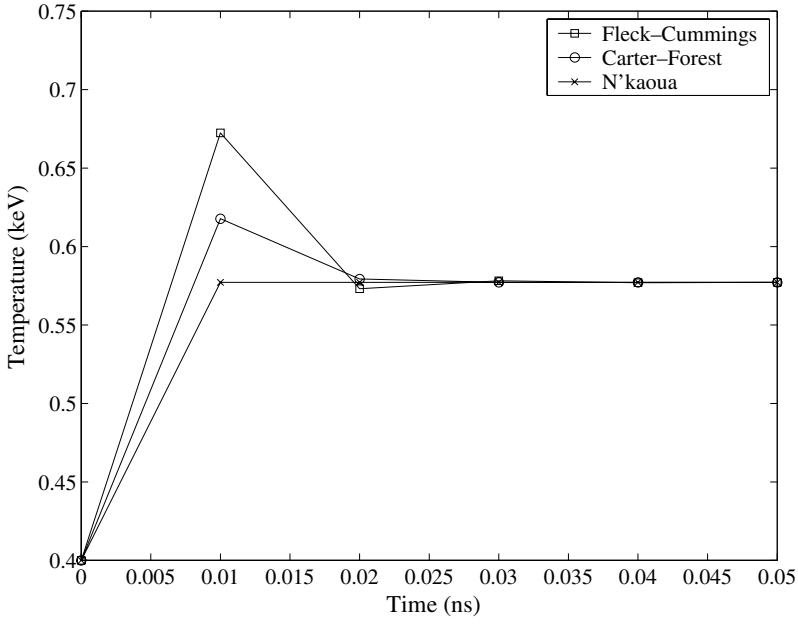

Fig. 2. Infinite medium material temperature, $T_R = 0.7$ keV.

immediately calculates the correct equilibrium solution after a single time step, regardless how far apart the material and radiation temperatures are initially. In Fig. 1, the Carter–Forest method nearly calculates the correct equilibrium solution after a single time step, and certainly yields the correct solution in the following

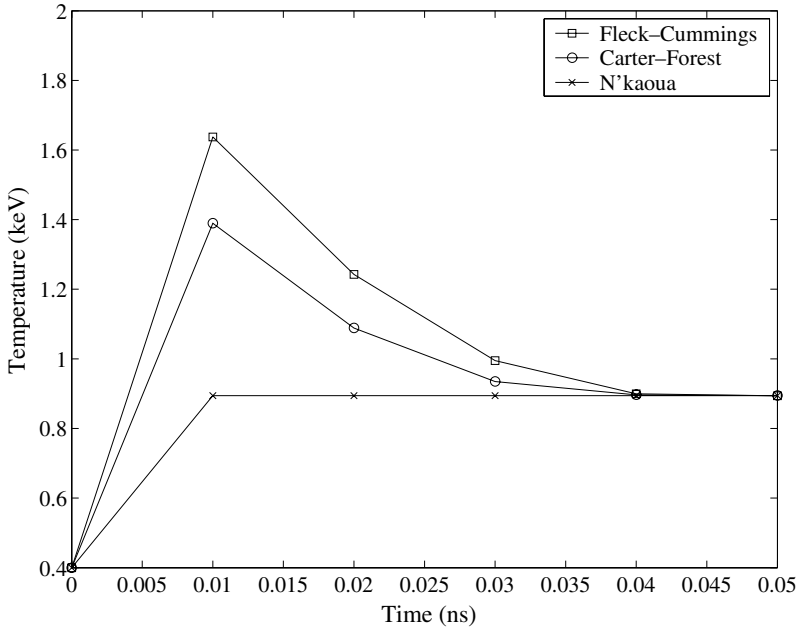

Fig. 3. Infinite medium material temperature, $T_R = 1.0$ keV.

time step. The Fleck–Cummings method oscillates unphysically, until the correct solution is calculated only at the end of several time steps. This behavior was also observed by Martin and Brown [15]. As the initial radiation temperature and material temperature increasingly differ, the Carter–Forest results become less accurate, requiring several time steps to calculate the correct equilibrium solution. We see in Fig. 3 that both the Fleck–Cummings and Carter–Forest methods overshoot the equilibrium solution, calculating the correct answer only after several time steps. This confirms our theoretical predictions that the N'kaoua method has the equilibrium diffusion limit, the Carter–Forest method has the equilibrium diffusion limit if the problem is initially near equilibrium, and the Fleck–Cummings method never has the equilibrium diffusion limit.

We now consider a more complex, space-dependent problem, consisting of a 0.25 cm one-dimensional slab initially at equilibrium at 1 keV. Since this problem is at equilibrium, there is no initial layer. However, this problem will serve to test the accuracy of each method's asymptotically generated diffusion equation. The problem has a reflective boundary condition on the left boundary and an incident Planckian source at 0.1 keV on the right boundary. Physically, at $t = 0$, the temperature of the slab begins to decrease as energy flows from the interior of the slab to the cooler outer boundary. Although a temperature gradient exists between the reflective left boundary and the exterior right boundary, the material and radiation should remain locally at equilibrium as the material cools.

We have simulated this problem using all three Monte Carlo methods, employing a 0.005 cm spatial grid, and implicit capture along the particle track length [10,12,19]. In our simulations, the spatial grid is optically thin (0.5 mean-free paths). Thus, the effects of spatial discretization should be negligible, as we assumed in our asymptotic analysis. In calculations using the Fleck–Cummings method, we again set the implicitness factor to $\alpha = 1$. We also use two separate time discretizations: a $\Delta t = 0.01$ ns fine grid, and a $\Delta t = 0.1$ ns coarse grid. We provide the fine-grid results as a reference for the less-accurate coarse-grid calculations, and not as a study in truncation error. Although the fine grid time-step size is much larger than the mean-free time of a photon in this problem, it was nonetheless sufficient to produce an accurate

solution. The fact that the Monte Carlo methods generated accurate solutions even though an optically small time step was not used points to the robustness of these methods. The coarse grid will serve as a test case for our asymptotic analysis results, since these time steps are definitely not optically small.

In Figs. 4–7, we plot the results of our simulations in the leftmost spatial cell ($x = \Delta x/2 = 0.0025$ cm) as a function of time. In Fig. 4, we have plotted the coarse Δt and fine Δt temperatures as a function of time for all of the three Monte Carlo methods considered. In Figs. 5–7, we have plotted aT^4 and the radiation energy density

$$E = \frac{1}{c}\int I \,\mathrm{d}\Omega \tag{97}$$

for the coarse time grid for each Monte Carlo method. In the equilibrium diffusion limit, E should be identical to aT^4. In Figs. 5–7 we also plot aT^4 for the fine time grid (solid line) as a reference.

From Fig. 4 (material temperature at $x = 0.0025$ cm for $0 \leqslant t \leqslant 1$ ns), we see that all three methods yield qualitatively accurate material temperatures, even when extremely large time steps are used. However, Fig. 4 shows that for the coarse time grid, the Carter–Forest solution is nearly exact for the coarse time grid, the errors in the Fleck–Cummings and N'kaoua temperatures are about 3% and 5%, respectively, at $t = 1$ ns. The relative accuracy of the Carter–Forest solution can be explained as follows.

Conceptually, the errors generated by the Fleck–Cummings, Carter–Forest, and N'kaoua methods are of two types: a *linearization error*, which occurs when the nonlinear problem is approximated by a linear problem during the time step, and a *truncation error*, which occurs when the linear problem is time-discretized (the time-dependent emission source is approximated). The Fleck–Cummings method contains both types of errors. The Carter–Forest method has the same linearization errors as the Fleck–Cummings, but because Carter–Forest solves the resulting linear equations exactly, it has no temporal truncation error.

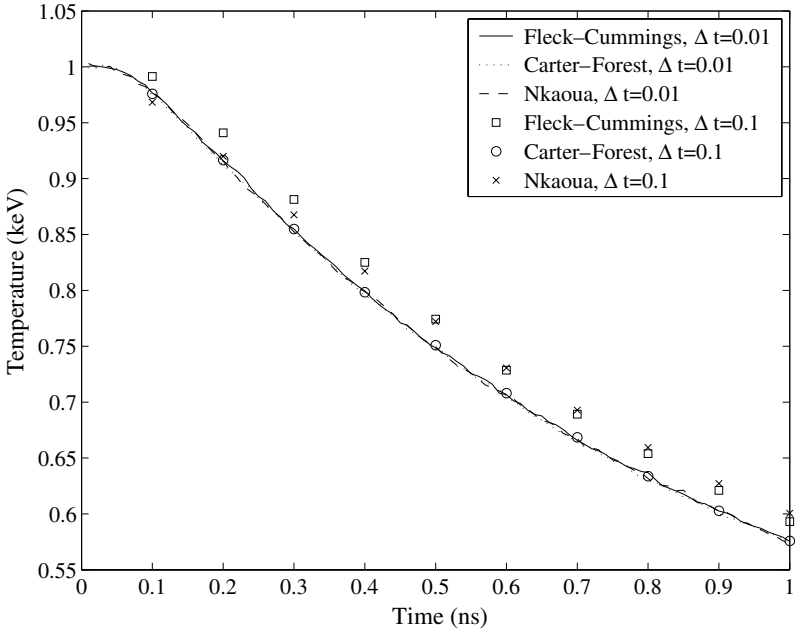

Fig. 4. Material temperature at $x = 0.0025$ cm.

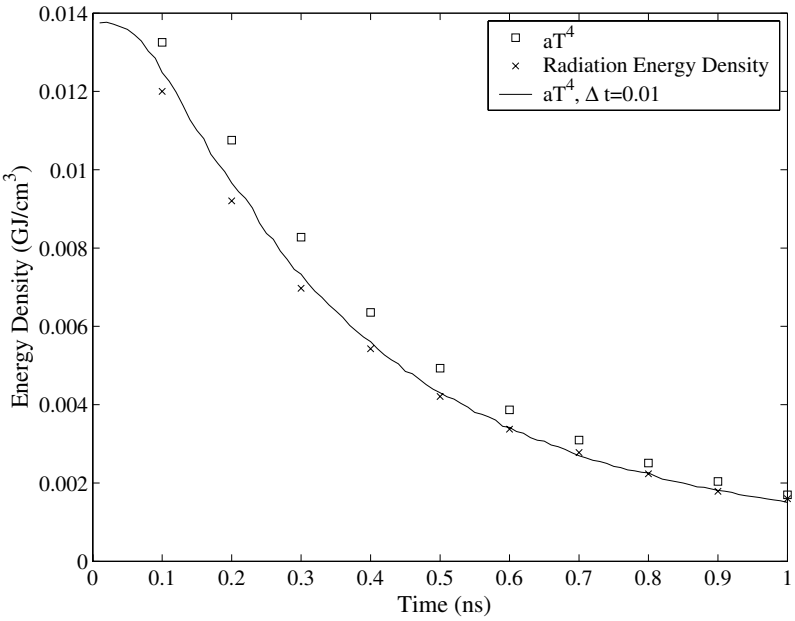

Fig. 5. Fleck–Cummings radiation energy density at $x = 0.0025$ cm.

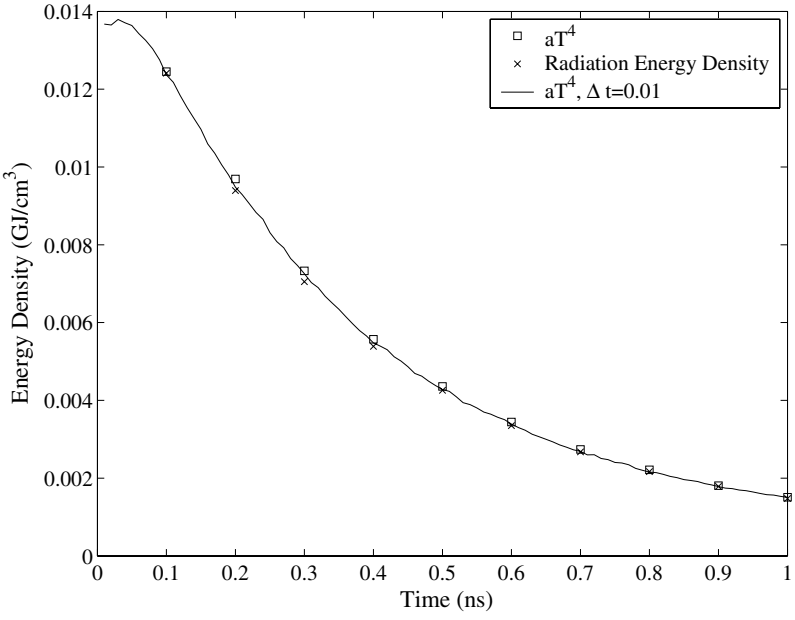

Fig. 6. Carter–Forest radiation energy density at $x = 0.0025$ cm.

The N'kaoua method is fundamentally different from the Fleck–Cummings and Carter–Forest methods; it is *almost* free of the linearization errors (it holds the opacity constant over a time step, as the other Monte Carlo methods do), but has a temporal truncation error (it approximates the emission source implicitly). The situation is summarized in Table 1.

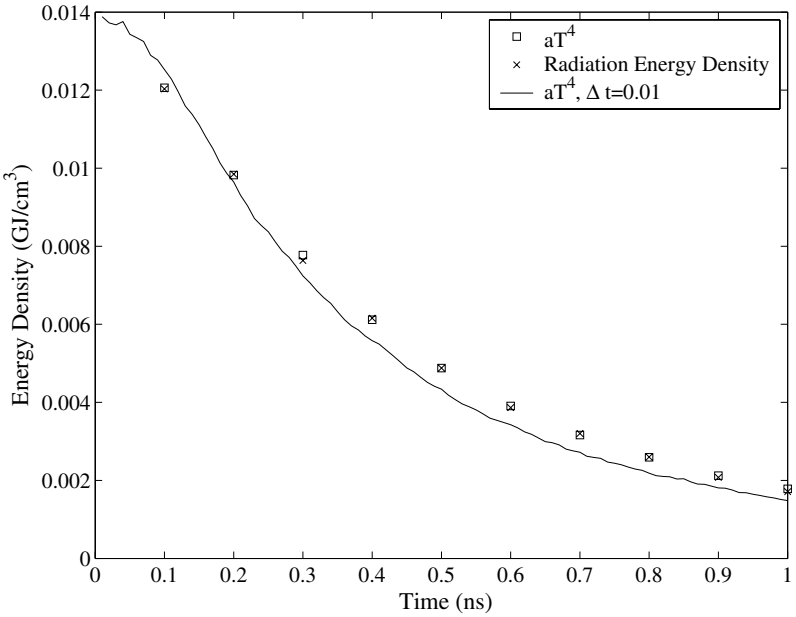

Fig. 7. N'kaoua radiation energy density at $x = 0.0025$ cm.

Table 1
Truncation and linearization errors

Monte Carlo method	Linearization error	Temporal truncation error
Fleck–Cummings	Yes	Yes
Carter–Forest	Yes	No
N'kaoua	No[a]	Yes

[a] Except for using a constant opacity over the time step.

It is now possible to explain why the Carter–Forest method is more accurate than the other methods in Fig. 4. First, the Carter–Forest and Fleck–Cummings methods have the same linearization errors, but the Fleck–Cummings method has an additional temporal truncation error. Therefore, the Carter–Forest method should generally be more accurate than the Fleck–Cummings method – and for this problem, it is. Also, for problems in which the temporal truncation error dominates the linearization error, Table 1 shows that the Carter–Forest method should be more accurate than the N'kaoua method. (Conversely, for problems in which the linearization error dominates the temporal truncation error, the N'kaoua method should be more accurate.) The fact that the Carter–Forest method is more accurate in Fig. 4 indicates that the underlying problem has larger truncation than linearization errors.

We now examine the radiation energy density calculated by each Monte Carlo method. Figs. 5–7 (aT^4 and E at $x = 0.0025$ cm for $0 \leqslant t \leqslant 1$ ns) show that – as predicted – the Fleck–Cummings solution is not in equilibrium ($E \neq aT^4$), the Carter–Forest solution is nearly in equilibrium ($E \approx aT^4$), and the N'kaoua solution is in equilibrium ($E = aT^4$). Again, the Carter–Forest solution is the most accurate, with errors in the Fleck–Cummings and N'kaoua values of E at about 6% and 16%, respectively, at $t = 0.1$ sh. We also see, from Fig. 5, that the unphysical behavior of the Fleck–Cummings method is temporary, and eventually the Fleck–Cummings solution reaches equilibrium.

Thus, for this spatially-dependent problem, the N'kaoua method has the equilibrium diffusion limit, and the Carter–Forest also has the equilibrium diffusion limit, since the material temperature does not change by much over a time step. The Fleck–Cummings method does not have the equilibrium diffusion limit, and unphysically produces a radiation energy density that is not in equilibrium with the material temperature. Nevertheless, even when optically large time steps are employed, all three Monte Carlo methods calculated fairly accurate material temperatures.

6. Conclusions

We have performed an asymptotic analysis for three Monte Carlo methods for grey radiative transfer, similar to the asymptotic analysis performed on deterministic transport methods. In this asymptotic limit, the mean-free path and mean-free time of a photon become small, the time discretization is fixed, and the timesteps become optically large. This analysis is of interest because in many problems it is computationally impractical to employ optically small time steps.

Our asymptotic analysis shows that (i) the N'kaoua method has the equilibrium diffusion limit, (ii) the Carter–Forest method has the equilibrium diffusion limit if the material temperature change during a time step is small, and (iii) the Fleck–Cummings method does not have the equilibrium diffusion limit. Thus, if a time discretization is chosen that is optically large, but nonetheless resolves the material temperature change, both the N'kaoua and Carter–Forest methods will produce accurate results, while the Fleck–Cummings method may calculate unphysical material temperatures and radiation intensities.

With a set of numerical results, we have demonstrated the applicability of our theoretical analysis. In an infinite medium problem with an unresolved initial layer, the N'kaoua method always produced accurate results, the Carter–Forest method produced accurate results if the radiation and material were not too far away from equilibrium initially, and the Fleck–Cummings method produced unphysical results. In a spatially-dependent problem initially in equilibrium, the N'kaoua and Carter–Forest methods retained temperature and radiation equilibrium, while the Fleck–Cummings method yielded a radiation intensity that was not in equilibrium with the material temperature. Nonetheless, all methods produced fairly accurate estimates of the material temperature.

Of the three Monte Carlo methods examined, the Fleck-Cummings method produced the most unphysical results in our numerical simulations. However, extremely large time steps were required for the Fleck–Cummings method to perform poorly. The Fleck–Cummings method gave accurate results if smaller, but still optically large, time steps were employed. Thus, the Fleck–Cummings method will not generate unphysical solutions for *all* problems with diffusive characteristics. This observation is consistent with our theoretical results, in which the asymptotic analysis of the Fleck–Cummings equations generated a diffusion equation, but did not require the radiation intensity and material temperature to be in local equilibrium. Also, from our numerical simulations, we have noted that the unphysical behavior of the Fleck–Cummings method is apparently temporary, and correct equilibrium solutions are eventually generated.

The theoretical and numerical results presented in this paper are consistent with conventional wisdom regarding the Fleck–Cummings method. This method, which has been used for many years to simulate thermal radiation transport, has known deficiencies when used with large time steps. For example, Fleck–Cummings simulations with large time steps can violate the maximum principle [14], which places bounds on the material temperature and radiation energy density. In practical problems, these inaccuracies are usually observed to be temporary; after a few time steps, they damp out and the numerical solution behaves in a more quantitatively correct manner. The analysis in this paper shows that in the asymptotic

equilibrium diffusion limit, the Fleck–Cummings method limits to a time-discretized equation that resembles – but is not – a time-discretized equilibrium diffusion equation. Among other things, this asymptotic Fleck–Cummings equation incorrectly does not force the radiation intensity and material temperature to be in local equilibrium. Our numerical results in fact show that lack of equilibrium in the Fleck–Cummings solution persists for several time steps. However, like the violations of the maximum principle, this unphysical error damps away after several time steps.

Overall, when a system is "hit" with a burst of radiation that rapidly drives it out of equilibrium, the Fleck–Cummings method *can* behave unphysically (violation of the maximum principle, unphysical oscillations, lack of equilibrium between radiation intensity and material temperature) for a few time steps; and then, afterward, settle into a more physically correct behavior. During these "transient" times, the Fleck–Cummings method is not guaranteed to generate accurate or physically correct solutions. If accurate solutions are required for all time steps and spatial points, then Fleck–Cummings solutions should receive very careful scrutiny in these "transient" parts of phase space.

The analysis and the numerical results in this paper demonstrate that for stressful diffusive problems, the Carter–Forest method is slightly more robust than the Fleck–Cummings method. However, in problems that are not near equilibrium, the Carter–Forest method can experience the same deficiencies as the Fleck–Cummings method. Also, the Carter–Forest method employs a Monte Carlo representation of the absorption-emission physics that is physically correct (if nonlinearities are ignored), in contrast to the Fleck–Cummings method, with its pseudo-scattering and pseudo-absorption. Thus, if the problem parameters are such that truncation errors are more important than linearization errors, the Carter–Forest method is capable of producing more accurate solutions than the Fleck–Cummings method.

We wish to emphasize that our analysis and results do not show that the Fleck–Cummings method is fatally flawed. However, this method does have weaknesses, some of them subtle. The aim of this paper is to analyze the strengths and weaknesses of the Fleck–Cummings, Carter–Forest, and N'kaoua methods in stressful, diffusive problems, so that these methods can be employed to solve practical problems with a better understanding of the errors that will inevitably occur.

In the analysis presented in this paper, we have examined only spatially continuous versions of each Monte Carlo method. In practical implementations, these methods employ a spatial discretization in which the material temperature (and temperature-dependent material properties) are calculated as cell-averaged quantities. In practical problems, the spatial cells cannot always be chosen to be optically thin. Thus, a complete asymptotic analysis would include the effects of spatial discretization. Also, the Carter–Forest and Fleck–Cummings methods may have an advantage over the N'kaoua method in problems with optically thick cells. Since the Fleck–Cummings and Carter–Forest methods employ effective scattering to model the absorption-reemission process, these cells will appear thick and highly scattering. Although inefficient (particles will experience many collisions during their lifetime), Monte Carlo simulation can treat cells of this type fairly accurately. However, the N'kaoua method does not employ effective scattering, which causes these cell to appear thick and highly absorbing [12]. This is a situation for which Monte Carlo simulation is not well suited. If analog tracking is employed, very few particles may be able to pass through the cell. If nonanalog simulation is used, the statistical noise of the calculation may be extremely high. Thus, if spatial discretization is considered, it is not clear that the N'kaoua method will outperform the Fleck–Cummings and Carter–Forest methods in problems near the equilibrium diffusion limit.

In addition to subdividing the problem into spatial cells, a piecewise-linear spatial representation of the emission source in each cell is often used in realistic problems [20]. This linear source may be important in the asymptotic analysis of spatially discretized problems. We have also specifically ignored boundary layers and initial-boundary layers, which may be important in some problems, and frequency-dependent problems. These issues remain for future work.

Acknowledgements

We wish to thank Todd Urbatsch and Tom Evans for their helpful comments. The work of the first author (JDD) was performed under U.S. Government contract W-7405-ENG-36 for Los Alamos National Laboratory, which is operated by the University of California for the U.S. Department of Energy.

Appendix A. Asymptotic analysis of the Fleck–Cummings and Carter–Forest methods

We now present detailed asymptotic analyses of both the Fleck–Cummings and Carter–Forest methods. These analyses yield the results presented in Section 4.

A.1. The Fleck–Cummings method

Applying the Fleck–Cummings approximation described previously to Eqs. (9) and (10), we obtain the interior equations

$$\frac{\epsilon^2}{c}\frac{\partial I^{(\mathrm{i})}}{\partial t}+\epsilon\vec{\Omega}\cdot\vec{\nabla}I^{(\mathrm{i})}+\sigma_n I^{(\mathrm{i})}=\frac{1}{4\pi}\sigma_{s,n}\int I^{(\mathrm{i})}\,\mathrm{d}\Omega+\frac{1}{4\pi}\sigma_{\mathrm{a},n}ac\left(T_n^{(\mathrm{i})}\right)^4 \tag{A.1}$$

and

$$\epsilon^2\frac{\partial}{\partial t}U_{\mathrm{m}}\left(T^{(\mathrm{i})}\right)=\sigma_{\mathrm{a},n}\left[\int I^{(\mathrm{i})}\,\mathrm{d}\Omega-ac\left(T_n^{(\mathrm{i})}\right)^4\right]. \tag{A.2}$$

In Eqs. (A.1) and (A.2), we have defined the pseudo-scattering opacity as

$$\sigma_{s,n}=\sigma_n\frac{\alpha\beta_n c\sigma_n\Delta t_n}{\epsilon^2+\alpha\beta_n c\sigma_n\Delta t_n} \tag{A.3}$$

and the pseudo-absorption opacity as

$$\sigma_{\mathrm{a},n}=\sigma_n\frac{\epsilon^2}{\epsilon^2+\alpha\beta_n c\sigma_n\Delta t_n}. \tag{A.4}$$

We note that $T_n^{(\mathrm{i})}$ in Eqs. (A.1) and (A.2) is the material temperature evaluated at the end of the previous time step. To simplify the following analysis, we have not integrated Eq. (A.2) over the time step. We can now perform an asymptotic analysis by comparing terms of the same order in ϵ. In this case, the pseudo-scattering opacity can be expanded as

$$\sigma_{s,n}=\sigma_n^{(0)}+\epsilon\sigma_n^{(1)}+\epsilon^2\sigma_{s,n}^{(2)}+\cdots \tag{A.5}$$

and the pseudo-absorption opacity as

$$\sigma_{\mathrm{a},n}=\epsilon^2\sigma_{\mathrm{a},n}^{(2)}+\cdots, \tag{A.6}$$

where

$$\sigma_{\mathrm{a},n}^{(2)}=\frac{1}{\alpha\beta_n^{(0)}c\Delta t_n}, \tag{A.7}$$

and

$$\sigma_{s,n}^{(2)} = \sigma_n^{(2)} - \sigma_{\mathrm{a},n}^{(2)}. \tag{A.8}$$

The O(1) equation is

$$\sigma_n^{(0)} I^{(\mathrm{i},0)} = \sigma_n^{(0)} \frac{1}{4\pi} \int I^{(\mathrm{i},0)} \,\mathrm{d}\Omega, \tag{A.9}$$

which can be written as

$$I^{(\mathrm{i},0)} = \frac{1}{4\pi} \phi^{(\mathrm{i},0)}. \tag{A.10}$$

Here $\phi^{(\mathrm{i},0)}$, the leading-order angularly-integrated intensity, is unspecified. Also, since the leading-order intensity is isotropic, the leading-order flux vanishes ($\vec{F}^{(\mathrm{i},0)} = 0$).

Next, the O(ϵ) equation is given by

$$\vec{\Omega} \cdot \vec{\nabla} I^{(\mathrm{i},0)} + \sigma_n^{(0)} I^{(\mathrm{i},1)} = \frac{1}{4\pi} \sigma_n^{(0)} \phi^{(\mathrm{i},1)}. \tag{A.11}$$

Using Eq. (A.10), Eq. (A.11) becomes

$$I^{(\mathrm{i},1)} = -\frac{1}{4\pi\sigma_n^{(0)}} \vec{\Omega} \cdot \vec{\nabla} \phi^{(\mathrm{i},0)} + \frac{1}{4\pi} \phi^{(\mathrm{i},1)}, \tag{A.12}$$

where $\phi^{(\mathrm{i},1)}$ is unspecified. Also, from Eq. (A.12), the O(ϵ) radiation flux is

$$\vec{F}^{(\mathrm{i},1)} = -\frac{1}{3\sigma_n^{(0)}} \vec{\nabla} \phi^{(\mathrm{i},0)}, \tag{A.13}$$

which is a statement of Fick's law.

The O(ϵ^2) equations are

$$\begin{aligned} &\frac{1}{c} \frac{\partial I^{(\mathrm{i},0)}}{\partial t} + \vec{\Omega} \cdot \vec{\nabla} I^{(\mathrm{i},1)} + \sigma_n^{(0)} I^{(\mathrm{i},2)} + \sigma_n^{(1)} I^{(\mathrm{i},1)} + \sigma_n^{(2)} I^{(\mathrm{i},0)} \\ &\quad = \frac{1}{4\pi} \left(\sigma_n^{(0)} \phi^{(\mathrm{i},2)} + \sigma_n^{(1)} \phi^{(\mathrm{i},1)} + \sigma_{s,n}^{(2)} \phi^{(\mathrm{i},0)} \right) + \frac{1}{4\pi} \sigma_{\mathrm{a},n}^{(2)} ac \left(T_n^{(\mathrm{i},0)} \right)^4, \end{aligned} \tag{A.14}$$

and

$$\frac{\partial}{\partial t} U_{\mathrm{m}} \left(T^{(\mathrm{i},0)} \right) = \sigma_{\mathrm{a},n}^{(2)} \left[\phi^{(\mathrm{i},0)} - ac \left(T_n^{(\mathrm{i},0)} \right)^4 \right]. \tag{A.15}$$

Integrating Eq. (A.14) over all directions, and using Eqs. (A.10) and (A.12), we obtain

$$\frac{1}{c} \frac{\partial \phi^{(\mathrm{i},0)}}{\partial t} - \vec{\nabla} \cdot \frac{1}{3\sigma_n^{(0)}} \vec{\nabla} \phi^{(\mathrm{i},0)} + \sigma_{\mathrm{a},n}^{(2)} \phi^{(\mathrm{i},0)} = \sigma_{\mathrm{a},n}^{(2)} ac \left(T_n^{(\mathrm{i},0)} \right)^4. \tag{A.16}$$

Eq. (A.16) is the diffusion equation for the leading-order interior intensity, Eq. (91).

Integrating Eq. (A.15) over the time step, and using Eq. (A.16), we obtain

$$\frac{U_{\mathrm{m}} \left(T_{n+1}^{(\mathrm{i},0)} \right) - U_{\mathrm{m}} \left[T^{(\mathrm{i},0)}(\vec{r}, t_n) \right]}{\Delta t_n} + \frac{1}{c} \frac{\phi_{n+1}^{(\mathrm{i},0)} - \phi^{(\mathrm{i},0)}(\vec{r}, t_n)}{\Delta t_n} = \frac{1}{\Delta t_n} \int_{t_n}^{t_{n+1}} \vec{\nabla} \cdot \frac{1}{3\sigma_n^{(0)}} \vec{\nabla} \phi^{(\mathrm{i},0)}(\vec{r}, t) \,\mathrm{d}t. \tag{A.17}$$

Here, $T_{n+1}^{(\mathrm{i},0)}$ and $\phi_{n+1}^{(\mathrm{i},0)}$ represent the leading-order material temperature and angularly-integrated radiation intensity at the end of the time step, respectively. We must now perform an initial-layer analysis to develop initial conditions for $T^{(\mathrm{i},0)}(\vec{r},t_n)$ and $\phi^{(\mathrm{i},0)}(\vec{r},t_n)$.

The equations for the initial layer are

$$\frac{\epsilon^2}{c}\frac{\partial I^{(\mathrm{il})}}{\partial t}+\frac{1}{c}\frac{\partial I^{(\mathrm{il})}}{\partial \tau}+\epsilon\vec{\Omega}\cdot\vec{\nabla}I^{(\mathrm{il})}+\sigma_n I^{(\mathrm{il})}=\frac{1}{4\pi}\sigma_{s,n}\int I^{(\mathrm{il})}\,\mathrm{d}\Omega+\frac{1}{4\pi}\sigma_{\mathrm{a},n}ac\left(T_n^{(\mathrm{i})}\right)^4 \tag{A.18}$$

and

$$\epsilon^2\frac{\partial}{\partial t}U_{\mathrm{m}}\left(T^{(\mathrm{il})}\right)+\frac{\partial}{\partial \tau}U_{\mathrm{m}}\left(T^{(\mathrm{il})}\right)=\sigma_{\mathrm{a},n}\left[\int I^{(\mathrm{il})}\,\mathrm{d}\Omega-ac\left(T_n^{(\mathrm{i})}\right)^4\right]. \tag{A.19}$$

The O(1) equations are given by

$$\frac{1}{c}\frac{\partial I^{(\mathrm{il},0)}}{\partial \tau}+\sigma_n^{(0)}I^{(\mathrm{il},0)}=\frac{1}{4\pi}\sigma_n^{(0)}\phi^{(\mathrm{il},0)} \tag{A.20}$$

and

$$\frac{\partial}{\partial \tau}U_{\mathrm{m}}\left(T^{(\mathrm{il},0)}\right)=0. \tag{A.21}$$

Integrating Eq. (A.20) over all directions, we have

$$\frac{1}{c}\frac{\partial \phi^{(\mathrm{il},0)}}{\partial \tau}=\frac{\partial}{\partial \tau}U_{\mathrm{m}}\left(T^{(\mathrm{il},0)}\right)=0, \tag{A.22}$$

and, to leading order, there is no initial layer for the material temperature or radiation intensity. The initial conditions for $T^{(\mathrm{i},0)}(\vec{r},t_n)$ and $\phi^{(\mathrm{i},0)}(\vec{r},t_n)$ are then given directly by the interior solutions at the end of the previous time step.

Using the results from the initial-layer analysis, Eq. (A.17) now becomes

$$\frac{U_{\mathrm{m}}\left(T_{n+1}^{(\mathrm{i},0)}\right)-U_{\mathrm{m}}\left(T_n^{(\mathrm{i},0)}\right)}{\Delta t_n}+\frac{1}{c}\frac{\phi_{n+1}^{(\mathrm{i},0)}-\phi_n^{(\mathrm{i},0)}}{\Delta t_n}=\frac{1}{\Delta t_n}\int_{t_n}^{t_{n+1}}\vec{\nabla}\cdot\frac{1}{3\sigma_n^{(0)}}\vec{\nabla}\phi^{(\mathrm{i},0)}(\vec{r},t)\,\mathrm{d}t. \tag{A.23}$$

This is the equation for the leading-order material temperature, Eq. (92).

A.2. The Carter–Forest method

Applying the Carter–Forest approximation to Eqs. (9) and (10), we obtain the interior equations

$$\frac{\epsilon^2}{c}\frac{\partial I^{(\mathrm{i})}}{\partial t}+\epsilon\vec{\Omega}\cdot\vec{\nabla}I^{(\mathrm{i})}+\sigma_n I^{(\mathrm{i})}=\frac{1}{4\pi}\sigma_n cU_{\mathrm{r}}^{(\mathrm{i})}, \tag{A.24}$$

$$\epsilon^2\frac{\partial U_{\mathrm{r}}^{(\mathrm{i})}}{\partial t}=\sigma_n\beta_n\left(\int I^{(\mathrm{i})}\,\mathrm{d}\Omega-cU_{\mathrm{r}}^{(\mathrm{i})}\right) \tag{A.25}$$

and

$$\epsilon^2\frac{\partial}{\partial t}U_{\mathrm{m}}\left(T^{(\mathrm{i})}\right)=\sigma_n\left(\int I^{(\mathrm{i})}\,\mathrm{d}\Omega-cU_{\mathrm{r}}^{(\mathrm{i})}\right). \tag{A.26}$$

To simplify the following analysis, we do not solve Eq. (A.25) and substitute into Eq. (A.24), nor do we integrate Eq. (A.26) over the time step. Also, we treat $U_{\mathrm{r}}^{(\mathrm{i})}$ as an unknown, and not as an explicit function of temperature.

We now proceed with an asymptotic analysis of the interior equations. The O(1) equations are

$$\sigma_n^{(0)} I^{(\mathrm{i},0)} = \frac{1}{4\pi}\sigma_n^{(0)} c U_{\mathrm{r}}^{(\mathrm{i},0)}, \tag{A.27}$$

$$0 = \sigma_n^{(0)}\beta_n^{(0)}\left(\phi^{(\mathrm{i},0)} - cU_{\mathrm{r}}^{(\mathrm{i},0)}\right) \tag{A.28}$$

and

$$0 = \sigma_n^{(0)}\left(\phi^{(\mathrm{i},0)} - cU_{\mathrm{r}}^{(\mathrm{i},0)}\right). \tag{A.29}$$

Eq. (A.27) can be written as

$$I^{(\mathrm{i},0)} = \frac{1}{4\pi} c U_{\mathrm{r}}^{(\mathrm{i},0)}, \tag{A.30}$$

which is consistent with Eqs. (A.28) and (A.29). Again, using Eq. (13), the leading-order interior radiation flux vanishes.

Next, the O(ϵ) equations are

$$\vec{\Omega}\cdot\vec{\nabla} I^{(\mathrm{i},0)} + \sigma_n^{(0)} I^{(\mathrm{i},1)} = \frac{1}{4\pi}\sigma_n^{(0)} c U_{\mathrm{r}}^{(\mathrm{i},1)}, \tag{A.31}$$

$$0 = \sigma_n^{(0)}\beta_n^{(0)}\left(\phi^{(\mathrm{i},1)} - cU_{\mathrm{r}}^{(\mathrm{i},1)}\right), \tag{A.32}$$

and

$$0 = \sigma_n^{(0)}\left(\phi^{(\mathrm{i},1)} - cU_{\mathrm{r}}^{(\mathrm{i},1)}\right). \tag{A.33}$$

Using Eq. (A.30), Eq. (A.31) becomes

$$I^{(\mathrm{i},1)} = -\frac{1}{4\pi\sigma_n^{(0)}}\vec{\Omega}\cdot\vec{\nabla}\phi^{(\mathrm{i},0)} + \frac{1}{4\pi} c U_{\mathrm{r}}^{(\mathrm{i},1)}, \tag{A.34}$$

which is consistent with Eqs. (A.32) and (A.33). The corresponding O(ϵ) interior radiation flux is

$$\vec{F}^{(\mathrm{i},1)} = -\frac{1}{3\sigma_n^{(0)}}\vec{\nabla}\phi^{(\mathrm{i},0)}, \tag{A.35}$$

which, as in the Fleck–Cummings method, is Fick's law.

The O(ϵ^2) equations are

$$\frac{1}{c}\frac{\partial I^{(\mathrm{i},0)}}{\partial t} + \vec{\Omega}\cdot\vec{\nabla} I^{(\mathrm{i},1)} + \sigma_n^{(0)} I^{(\mathrm{i},2)} + \sigma_n^{(1)} I^{(\mathrm{i},1)} = \frac{1}{4\pi} c\left(\sigma_n^{(0)} U_{\mathrm{r}}^{(\mathrm{i},2)} + \sigma_n^{(1)} U_{\mathrm{r}}^{(\mathrm{i},1)}\right), \tag{A.36}$$

$$\frac{\partial U_{\mathrm{r}}^{(\mathrm{i},0)}}{\partial t} = \sigma_n^{(0)}\beta_n^{(0)}\left(\phi^{(\mathrm{i},2)} - cU_{\mathrm{r}}^{(\mathrm{i},2)}\right), \tag{A.37}$$

and

$$\frac{\partial}{\partial t}U_{\mathrm{m}}\left(T^{(\mathrm{i},0)}\right)=\sigma_n^{(0)}\left(\phi^{(\mathrm{i},2)}-cU_{\mathrm{r}}^{(\mathrm{i},2)}\right). \tag{A.38}$$

Integrating Eq. (A.36) over all directions, and using Eqs. (A.30), (A.34) and (A.37), we obtain

$$\frac{1}{c}\left(1+\frac{1}{\beta_n^{(0)}}\right)\frac{\partial\phi^{(\mathrm{i},0)}}{\partial t}=\vec{\nabla}\cdot\frac{1}{3\sigma_n^{(0)}}\vec{\nabla}\phi^{(\mathrm{i},0)}. \tag{A.39}$$

Eq. (A.39) is the diffusion equation for the leading-order interior radiation intensity, Eq. (93).

Next, integrating Eq. (A.38) over the time step, and using Eqs. (A.30), (A.37) and (A.39), yields

$$\frac{U_{\mathrm{m}}\left(T_{n+1}^{(\mathrm{i},0)}\right)-U_{\mathrm{m}}\left[T^{(\mathrm{i},0)}(\vec{r},t_n)\right]}{\Delta t_n}+\frac{1}{c}\frac{\phi_{n+1}^{(\mathrm{i},0)}-\phi^{(\mathrm{i},0)}(\vec{r},t_n)}{\Delta t_n}=\frac{1}{\Delta t_n}\int_{t_n}^{t_{n+1}}\vec{\nabla}\cdot\frac{1}{3\sigma_n^{(0)}}\vec{\nabla}\phi^{(\mathrm{i},0)}(\vec{r},t)\,\mathrm{d}t. \tag{A.40}$$

As with the Fleck–Cummings analysis, $T_{n+1}^{(\mathrm{i},0)}$ and $\phi_{n+1}^{(\mathrm{i},0)}$ are the leading-order material temperature and angularly-integrated radiation intensity at the end of the time step. We now perform an initial-layer analysis to develop expressions for $T^{(\mathrm{i},0)}(\vec{r},t_n)$ and $\phi^{(\mathrm{i},0)}(\vec{r},t_n)$.

The equations for the initial layer are

$$\frac{\epsilon^2}{c}\frac{\partial I^{(\mathrm{il})}}{\partial t}+\frac{1}{c}\frac{\partial I^{(\mathrm{il})}}{\partial\tau}+\epsilon\vec{\Omega}\cdot\vec{\nabla}I^{(\mathrm{il})}+\sigma_n I^{(\mathrm{il})}=\frac{1}{4\pi}\sigma_n cU_{\mathrm{r}}^{(\mathrm{il})}, \tag{A.41}$$

$$\epsilon^2\frac{\partial U_{\mathrm{r}}^{(\mathrm{il})}}{\partial t}+\frac{\partial U_{\mathrm{r}}^{(\mathrm{il})}}{\partial\tau}=\sigma_n\beta_n\left(\int I^{(\mathrm{il})}\,\mathrm{d}\Omega-cU_{\mathrm{r}}^{(\mathrm{il})}\right), \tag{A.42}$$

and

$$\epsilon^2\frac{\partial}{\partial t}U_{\mathrm{m}}\left(T^{(\mathrm{il})}\right)+\frac{\partial}{\partial\tau}U_{\mathrm{m}}\left(T^{(\mathrm{il})}\right)=\sigma_n\left(\int I^{(\mathrm{il})}\,\mathrm{d}\Omega-cU_{\mathrm{r}}^{(\mathrm{il})}\right). \tag{A.43}$$

The O(1) equations are

$$\frac{1}{c}\frac{\partial I^{(\mathrm{il},0)}}{\partial\tau}+\sigma_n^{(0)}I^{(\mathrm{il},0)}=\frac{1}{4\pi}\sigma_n^{(0)}cU_{\mathrm{r}}^{(\mathrm{il},0)}, \tag{A.44}$$

$$\frac{\partial U_{\mathrm{r}}^{(\mathrm{il},0)}}{\partial\tau}=\sigma_n^{(0)}\beta_n^{(0)}\left(\phi^{(\mathrm{il},0)}-cU_{\mathrm{r}}^{(\mathrm{il},0)}\right), \tag{A.45}$$

and

$$\frac{\partial}{\partial\tau}U_{\mathrm{m}}\left(T^{(\mathrm{il},0)}\right)=\sigma_n^{(0)}\left(\phi^{(\mathrm{il},0)}-cU_{\mathrm{r}}^{(\mathrm{il},0)}\right). \tag{A.46}$$

Integrating Eq. (A.44) over all directions, and combining the results with Eqs. (A.45) and (A.46), we obtain

$$-\frac{1}{c}\frac{\partial\phi^{(\mathrm{il},0)}}{\partial\tau}=\frac{1}{\beta_n^{(0)}}\frac{\partial U_{\mathrm{r}}^{(\mathrm{il},0)}}{\partial\tau}=\frac{\partial}{\partial\tau}U_{\mathrm{m}}\left(T^{(\mathrm{il},0)}\right). \tag{A.47}$$

Next, using Eqs. (55)–(58), the initial condition for $U_{\mathrm{r}}^{(\mathrm{il},0)}$,

$$U_{\mathrm{r}}^{(\mathrm{il},0)}(\vec{r},t_n,0) = a\left[T^{(0)}(\vec{r},t_n)\right]^4, \tag{A.48}$$

and the matching condition for $U_{\mathrm{r}}^{(\mathrm{il},0)}$,

$$\lim_{\tau\to\infty} U_{\mathrm{r}}^{(\mathrm{il},0)}(\vec{r},t,\tau) = U_{\mathrm{r}}^{(\mathrm{i},0)}(\vec{r},t), \tag{A.49}$$

we set $t = t_n$ and integrate Eq. (A.47) from $\tau = 0$ to $\tau = \infty$. We then have

$$\begin{aligned} -\frac{1}{c}\left[\phi^{(\mathrm{i},0)}(\vec{r},t_n) - \phi^{(0)}(\vec{r},t_n)\right] &= \frac{1}{\beta_n^{(0)}}\left\{U_{\mathrm{r}}^{(\mathrm{i},0)}(\vec{r},t_n) - a\left[T^{(0)}(\vec{r},t_n)\right]^4\right\} \\ &= U_{\mathrm{m}}\left[T^{(\mathrm{i},0)}(\vec{r},t_n)\right] - U_{\mathrm{m}}\left[T^{(0)}(\vec{r},t_n)\right], \end{aligned} \tag{A.50}$$

where $T^{(0)}(\vec{r},t_n)$ and $\phi^{(0)}(\vec{r},t_n)$ are the leading order temperature and angularly-integrated radiation intensity at the end of the previous time step. Using Eq. (A.30), the initial condition for the leading-order radiation intensity is given by

$$\phi^{(\mathrm{i},0)}(\vec{r},t_n) = \frac{\beta_n^{(0)}}{1+\beta_n^{(0)}}\phi^{(0)}(\vec{r},t_n) + \frac{1}{1+\beta_n^{(0)}}ac\left[T^{(0)}(\vec{r},t_n)\right]^4. \tag{A.51}$$

Also, from Eq. (A.50), the initial condition for the leading-order temperature is

$$U_{\mathrm{m}}\left[T^{(\mathrm{i},0)}(\vec{r},t_n)\right] = U_{\mathrm{m}}\left[T^{(0)}(\vec{r},t_n)\right] + \frac{1}{c}\left[\phi^{(0)}(\vec{r},t_n) - \phi^{(\mathrm{i},0)}(\vec{r},t_n)\right]. \tag{A.52}$$

These are the initial conditions given in the main text, Eqs. (94) and (95).

Using Eq. (A.52), Eq. (A.40) becomes

$$\frac{U_{\mathrm{m}}\left(T_{n+1}^{(\mathrm{i},0)}\right) - U_{\mathrm{m}}\left(T_n^{(\mathrm{i},0)}\right)}{\Delta t_n} + \frac{1}{c}\frac{\phi_{n+1}^{(\mathrm{i},0)} - \phi_n^{(\mathrm{i},0)}}{\Delta t_n} = \frac{1}{\Delta t_n}\int_{t_n}^{t_{n+1}} \vec{\nabla}\cdot\frac{1}{3\sigma_n^{(0)}}\vec{\nabla}\phi^{(\mathrm{i},0)}\,\mathrm{d}t, \tag{A.53}$$

where we have used that the leading-order solutions at the end of the previous times step are the corresponding interior solutions [i.e. $T^{(0)}(\vec{r},t_n) = T_n^{(\mathrm{i},0)}(\vec{r})$ and $\phi^{(0)}(\vec{r},t_n) = \phi_n^{(\mathrm{i},0)}(\vec{r})$]. Eq. (A.53) is the equation for the leading-order interior material temperature, Eq. (96).

We now discuss a case in which the Carter–Forest method nearly yields the equilibrium diffusion limit. Integrating Eq. (A.39) over the time step, and combining the results with Eq. (A.53), we have

$$U_{\mathrm{m}}\left(T_{n+1}^{(\mathrm{i},0)}\right) - U_{\mathrm{m}}\left(T_n^{(\mathrm{i},0)}\right) + \frac{1}{c}\left(\phi_{n+1}^{(\mathrm{i},0)} - \phi_n^{(\mathrm{i},0)}\right) = \frac{1}{c}\left(1+\frac{1}{\beta_n^{(0)}}\right)\left(\phi_{n+1}^{(\mathrm{i},0)} - \phi^{(\mathrm{i},0)}(\vec{r},t_n)\right). \tag{A.54}$$

Then, using Eq. (A.51), Eq. (A.54) can be simplified as

$$\beta_n^{(0)}\left[U_{\mathrm{m}}\left(T_{n+1}^{(\mathrm{i},0)}\right) - U_{\mathrm{m}}\left(T_n^{(\mathrm{i},0)}\right)\right] = \frac{\phi_{n+1}^{(\mathrm{i},0)}}{c} - a\left(T_n^{(\mathrm{i},0)}\right)^4. \tag{A.55}$$

Using Eq. (21), and assuming that the material temperature changes by a small amount over the time step, the left-hand side of Eq. (A.55) becomes

$$\frac{4a\left(T_n^{(\mathrm{i},0)}\right)^3}{C_{\mathrm{v}}\left(T_n^{(\mathrm{i},0)}\right)}\left[U_{\mathrm{m}}\left(T_{n+1}^{(\mathrm{i},0)}\right) - U_{\mathrm{m}}\left(T_n^{(\mathrm{i},0)}\right)\right] \approx 4a\left(T_n^{(\mathrm{i},0)}\right)^3\left(T_{n+1}^{(\mathrm{i},0)} - T_n^{(\mathrm{i},0)}\right) \approx a\left(T_{n+1}^{(\mathrm{i},0)}\right)^4 - a\left(T_n^{(\mathrm{i},0)}\right)^4. \tag{A.56}$$

From Eqs. (A.55) and (A.56), the leading-order radiation intensity at the end of the time step is

$$\phi_{n+1}^{(\mathrm{i},0)} = ac\left(T_{n+1}^{(\mathrm{i},0)}\right)^4, \tag{A.57}$$

which is an approximation to Eq. (11). Then, for all but the first time step, Eq. (A.53) can be approximated as

$$\frac{U_{\mathrm{m}}\left(T_{n+1}^{(\mathrm{i},0)}\right) - U_{\mathrm{m}}\left(T_n^{(\mathrm{i},0)}\right)}{\Delta t_n} + a\frac{\left(T_{n+1}^{(\mathrm{i},0)}\right)^4 - \left(T_n^{(\mathrm{i},0)}\right)^4}{\Delta t_n} = \frac{1}{\Delta t_n}\int_{t_n}^{t_{n+1}} \vec{\nabla}\cdot\frac{1}{3\sigma_n^{(0)}}\vec{\nabla}\phi^{(\mathrm{i},0)}\,\mathrm{d}t. \tag{A.58}$$

Eq. (A.58) is discretized version of Eq. (12). From Eq. (A.30), if the problem is at equilibrium at the end of the previous time step, then the initial layer for the radiation intensity vanishes. Then, the right hand side of Eq. (A.58) is the average radiation flux as the radiation intensity moves from $\phi_n^{(\mathrm{i},0)} = ac\left(T_n^{(\mathrm{i},0)}\right)^4$ to $\phi_{n+1}^{(\mathrm{i},0)} = ac\left(T_{n+1}^{(\mathrm{i},0)}\right)^4$.

For the first time step, we define an effective temperature $T_0^{(\mathrm{i},0)}$ such that Eq. (A.51) becomes

$$ac\left(T_0^{(\mathrm{i},0)}\right)^4 = \frac{\beta(T_i)}{1+\beta(T_i)}\phi_i + \frac{1}{1+\beta(T_i)}acT_i^4, \tag{A.59}$$

where ϕ_i and T_i are given by Eqs. (7) and (8), respectively. Using Eq. (21), Eq. (A.59) can be written as

$$ac\left(T_0^{(\mathrm{i},0)}\right)^4 + \frac{C_{\mathrm{v}}(T_i)}{4aT_i^3}\left[ac\left(T_0^{(\mathrm{i},0)}\right)^4 - acT_i^4\right] = \phi_i. \tag{A.60}$$

Then, if the difference between $T_0^{(\mathrm{i},0)}$ and T_i is small, we can use Eq. (A.56) to rewrite Eq. (A.60) as

$$U_{\mathrm{m}}\left(T_0^{(\mathrm{i},0)}\right) + a\left(T_0^{(\mathrm{i},0)}\right)^4 = U_{\mathrm{m}}(T_i) + \frac{1}{c}\phi_i. \tag{A.61}$$

Eq. (A.61) is identical to Eq. (15), the initial condition for the equilibrium diffusion equation. In addition, using Eqs. (A.53) and (A.57), we note that Eq. (A.58) will hold if $T_n^{(\mathrm{i},0)}$ for $n = 0$ is defined by Eq. (A.61).

References

[1] E.W. Larsen, The asymptotic diffusion limit of discretized transport problems, Nucl. Sci. Eng. 112 (1992) 336.
[2] E.W. Larsen, J.B. Keller, Asymptotic solution of neutron transport problems for small mean free paths, J. Math. Phys. 15 (1974) 75.
[3] G.J. Habetler, B.J. Matkowsky, Uniform asymptotic expansions in transport theory with small mean free paths, and the diffusion approximation, J. Math. Phys. 16 (1975) 846.
[4] E.W. Larsen, Diffusion theory as an asymptotic limit of transport theory for nearly critical systems with small mean free paths, Ann. Nucl. Energy 7 (1980) 249.
[5] E.W. Larsen, J.E. Morel, Warren F. Miller Jr., Asymptotic solutions of numerical transport problems in optically thick, diffusive regimes, J. Comput. Phys. 69 (1987) 283.
[6] E.W. Larsen, J.E. Morel, Asymptotic solutions of numerical transport problems in optically thick, diffusive regimes II, J. Comput. Phys. 83 (1989) 212.
[7] E.W. Larsen, G.C. Pomraning, V.C. Badham, Asymptotic analysis of radiative transfer problems, J. Quant. Spectrosc. Radiat. Transfer 29 (1983) 285.
[8] J.E. Morel, T.A. Wareing, K. Smith, A linear-discontinuous spatial differencing scheme for S_n radiative transfer calculations, J. Comput. Phys. 128 (1996) 445.
[9] M.L. Adams, P.F. Nowak, Asymptotic analysis of a computational method for time- and frequency-dependent radiative transfer, J. Comput. Phys. 146 (1998) 366.

[10] J.A. Fleck Jr., J.D. Cummings, An implicit Monte Carlo scheme for calculating time and frequency dependent radiation transport, J. Comput. Phys. 8 (1971) 313.
[11] L.L. Carter, C.A. Forest, Nonlinear radiation transport simulation with an implicit Monte Carlo method, LA-5038, Los Alamos National Laboratory, 1973 (unpublished).
[12] T. N'kaoua, Solution of the nonlinear radiative transfer equations by a fully implicit matrix Monte Carlo method coupled with the Rosseland diffusion equation via domain decomposition, SIAM J. Sci. Stat. Comput. 12 (1991) 505.
[13] G.C. Pomraning, The Equations of Radiation Hydrodynamics, Pergamon, Oxford, 1973.
[14] E.W. Larsen, B. Mercier, Analysis of a Monte Carlo method for nonlinear radiative transfer, J. Comput. Phys. 71 (1987) 50.
[15] W.R. Martin, F.B. Brown, Error modes in implicit Monte Carlo, Trans. Amer. Nucl. Soc. 85 (2001) 329.
[16] J.D. Densmore, E.W. Larsen, Maximum principle analysis of Monte Carlo methods for grey radiative transfer, in: Proceedings of the Mathematics and Computation 2003: A Century in Review, a Century Anew, Gatlinburg, TN, April 7–10, 2003.
[17] G.C. Pomraning, Initial and boundary conditions for equilibrium diffusion theory, J. Quant. Spectrosc. Radiat. Transfer 36 (1986) 69.
[18] E.D. Brooks III, Symbolic implicit Monte Carlo, J. Comput. Phys. 83 (1989) 433.
[19] F.B. Brown, W.R. Martin, Improved method for implicit Monte Carlo, Trans. Amer. Nucl. Soc. 86 (2002) 212.
[20] J.A. Fleck Jr., E.H. Canfield, A random walk procedure for improving the computational efficiency of the implicit Monte Carlo method for nonlinear radiation transport, J. Comput. Phys. 54 (1984) 508.